Soft robotics for physical simulators, artificial organs and implantable assistive devices

Received xxxxxx
Accepted for publication xxxxxx
Published xxxxxx

Abstract

In recent years, soft robotics technologies enabled the development of a new generation of biomedical devices. The combination of elastomeric materials with tunable properties and muscle-like motions paved the way towards more realistic phantoms and innovative soft active implants as artificial organs or assistive mechanisms. This review collects the most relevant studies performed towards the development of the above-mentioned devices in all the body systems, giving some insights about their distribution in the past 10 years, their level of development, and opening a discussion about the most commonly employed actuating technologies. The reported results show some promising trends, highlighting that the soft robotics approach can be useful in replicating particular material characteristics, in the case of static or passive organs, but also in reproducing specific natural motion patterns for the realization of dynamic phantoms or implants. At the same time, some important challenges still need to be addressed. However, joining forces with other research fields and disciplines, it will be possible to get one step closer to the realization of complex, active, self-sensing and deformable structures able to replicate as closely as possible the typical properties and functionalities of our natural body organs.

Keywords: soft robotics, physical simulators, artificial organs, implantable assistive devices, soft mechatronics

Introduction

In the last 10 years, soft robotics has introduced a new way of thinking about robots. Intrinsic safety, adaptability, resilience, and conformability are among the major advantages brought by the use of soft and flexible materials for the robot body. This trend is also influenced by the increasing awareness of how powerful biomimetics may be in obtaining better performances in robotics. However, although nature is one of the most creative designers, its optimality criteria, unlike engineering, respond to specific targets as survival or reproduction. For this reason, biomimetics should always aim at identifying the underlying functional principles, and not necessarily to copy the natural models. There is, however, a specific scientific field where this paradigm does not necessarily hold: where the reproduction of body organs and system functionalities using materials with comparable mechanical properties is of paramount importance; where any sudden geometrical or mechanical discontinuity may represent not just a possible source of failure, but also a limited chance of survival of a patient. This is the field of artificial organs and simulators of body parts. Although soft robotics is still considered at an early stage of development, it is already considered an appropriate technological candidate for all those biomedical applications, where safe and delicate, yet effective, interactions are necessary. Assistive and rehabilitation technologies, surgical instruments, prosthetic devices are the most promising fields where a transformational impact is expected already in the short/medium term. However, the most farsighted challenge remains the possibility to recreate and fully substitute organ functionalities. The research path that leads to achieve this goal is notoriously extremely complex. An artificial organ does not allow compromises: a system that does not fully meet all the physiological requirements is useless. For this reason, in some cases, research groups prefer to start the process with a simpler approach, focusing on the reproduction of organ functionalities without aiming at implantability. This is the case of physical body simulators: where scale, durability and biocompatibility are not a major concern, as they are used as platforms to support advanced medical training (high-fidelity

functional phantoms), to benchmark medical devices or to study and simulate the effect of specific physio-pathological conditions. They, indeed, represent a valuable alternative solution to the current approaches that are very limited due to their invasiveness (*in vivo* studies) or due to the complexity of dealing with excised tissues, namely their short life (*ex vivo* studies).

In this review, we focused our research on the latest advancements achieved in the field of soft robotics applied to artificial organs, physical simulators and implantable assistive devices. To pursue this objective, a total of 235 articles were reviewed ranged from 2001 to 2021. Among them, 142 original research papers published within the last five years are summarized, in terms of anatomical reproduction, materials, fabrication methods, performances, limits and challenges, and reported in the Supplementary Material, to highlight the latest achievements through the soft robotics approach. We, indeed, included all the studies where the use of soft materials and/or soft mechatronics represented the core enabling technology for the reproduction of specific properties, as geometry, appearance, and mechanical characteristics of both passive and active devices.

We took into consideration different body systems, underlining the current state of the art and the most recent advancements for each of them. We highlight which are the soft robotic artificial organs closest to clinical applications, and which are the most important challenges that are currently limiting a smooth development, ranging from the device long-lasting properties to biocompatibility.

Soft robotic physical simulators

The field of robotics applied to healthcare is constantly growing. Robotic simulators of human physiology provide powerful platforms to advance the development of novel treatments, prostheses, and therapies. The simulation of human body parts with materials similar to human tissues and with life-like abilities represents an emergent application field for Soft Robotics (1) that allows the development of artificial organs more and more similar to the natural counterpart in replicating all the mechanical characteristics and its functionality.

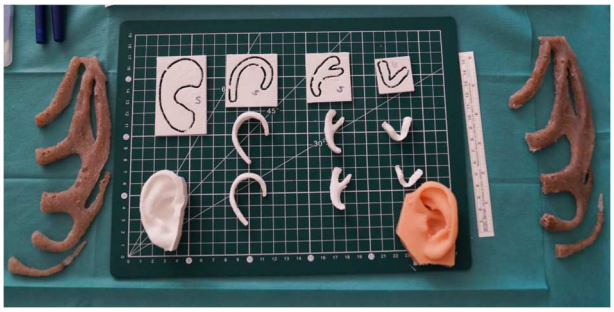

Figure 1 Ear static simulator. Courtesy of Dr. Elisa Mussi, Department of Industrial Engineering, University of Florence.

In this review, we categorized the synthetic simulators in static and dynamic simulators. The static simulators are made of soft and deformable materials, but the natural movements are not replicated. In the dynamic simulators, an actuation technology is introduced to simulate the physiological movements of the organ or tissue. While the dynamic passive simulators are moved by the surrounding conditions of pressure or flow, the dynamic active simulators integrate actuators that actively move the parts of interest, aiming at replicating the physiology.

1. *Static synthetic simulators*

Static phantoms have been widely employed for the development of systems able to help surgeons during training, pre-operative rehearsal or to study patient-specific conditions. Moreover, sometimes became extremely useful also for validating imaging techniques or algorithms.

Sensory organs

Within the group of organs responsible of sensory responses, researchers presented static phantoms of the ear.

Carving an auricular cartilage framework from autogenous cartilage—the most common technique for auricular reconstruction—is, indeed, one of the most challenging skills for the reconstructive surgeon to learn. Surgical simulation with highly realistic phantoms may assist with skill attainment. A rib cartilage model can also help experienced surgeons refine their carving skills and prepare for complex cases. In this framework, two studies have attempted face this challenge by reproducing an ear simulator to train surgeons in the development of an “aesthetic eye” able to identify proportions and harmonies and gain technical skills. In (2) starting from a case study, the preoperative simulation and planning process were analyzed with the objective to develop an interactive procedure, exploiting reverse engineering and additive manufacturing techniques, that can be accessed directly by the medical staff to create patient-specific simulators (see Figure 1 (2)). In another study (3), the costal cartilage model of a pediatric patient was developed using a high-resolution Computed Tomography (CT) scan from an 8-year-old boy. In both studies, simulators are made in silicone that are able to replicate the patient’s cartilages. Another important advantage of developing an ear simulator is the possibility to familiarize with the patient’s specific anatomy, which leads to a higher confidence of the surgeon in the operating room and the optimization of the costal cartilage harvesting phase, minimizing the invasiveness of the surgery. However, the applications of ear simulators can be various. Indeed, in (4) the design and development of silicone-based low -cost binaural ears on a Styrofoam based mannequin were presented, which were used for both multiple spatial audio applications and head related impulse response measurements.

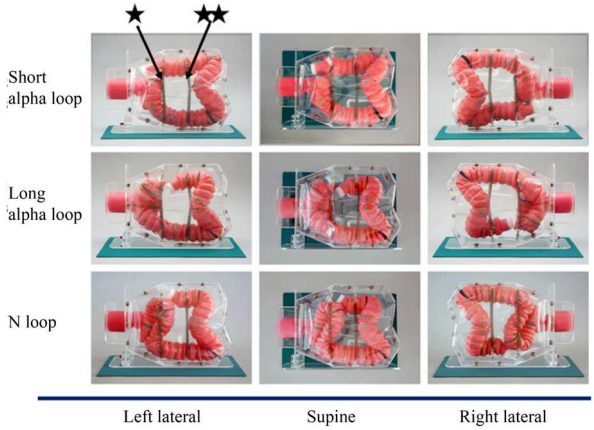

Figure 2 Intestine static simulator, introducing sigmoid and transverse colon suspensory attachment (star and double star) that combined with the transparent membrane decreases the possibility of phantom motion. Republished from (7).

Digestive system

Considering the digestive system, soft robotic technologies paved the way also towards the development of more realistic intestine phantoms for colonoscopy training. Colorectal cancer is, indeed, the third cancer with highest incidence worldwide. (5) Screening tests, as colonoscopy, help in finding early-stage polyps before they turn into cancer, reducing the mortality of the disease. Training the operators is therefore the best strategy to achieve high success rates in the afore-mentioned procedures. Since 1969, many simulators were presented (6). In fact, at present it is possible to find on the market extremely realistic phantoms made of silicone resin. This is the case of phantoms produced by the Kyoto Kagaku company, see Figure 2. These models were, in fact, casted (7). Upon CT data acquisitions, using a colored silicone mixture that provided an important visual accuracy to the systems. The different models present an increasing complexity of the system: apart from the different positions from where it is possible to practice colonoscopy, the M40 model presents the possibility to simulate the pressure of the anus, and a rigid but anthropomorphic casing (8), while the NKS (9), instead, is enclosed within a box characterized by transparent walls. However, the cost of such systems is high therefore also cheaper options were investigated. As a matter of fact, some researchers tried to replicate the structure of the intestine with off-the-shelf and inexpensive materials as fabric, e.g. red satin fabric (10), woven fabric (11) or by just using the transparent cover of a surgical sonographic probe (12), replicating the haustral folds with constraining elements, as rubber bands. Also, these alternatives showed promising results in improving the endoscopic skills of the surgeons.

Soft and anatomically accurate liver phantoms were studied for the medical training on liver minimally invasive procedures, such as transhepatic puncturing or endoscopic retrograde cholangiodrainage. During transhepatic surgery, needle localization is the most important parameter to be monitored under real-time Ultrasound (US) imaging guidance since it directly relates to the surgical outcome and patient safety. A soft silicone liver phantom with anatomically accurate biliary system and advanced sensorization enabled the interactive surgical training, giving quantitative information with high temporal and spatial resolution on the needle position during the simulated surgical procedure (13). The described phantom resembled a real liver also under endoscopy and computer tomography imaging. The phantom material composition was studied to match the ultrasound attenuation coefficients of the natural liver (14). Besides efforts were made to replicate the echoic properties of different liver lesions and anatomical districts, such as the parenchyma and the veins, the speed of sound in the simulated materials was out of range, leading to distorted US images (15). Gel-based synthetic materials that have comparable appearance to the natural liver parenchyma, portal veins and tumor lesions under US, CT and Magnetic Resonance Imaging (MRI) were studied in (16), however, a liver phantom that combines the multimodality imaging with anatomic realism requires further research (17).

Urinary system

Also, within the urinary system some organs, as kidney, prostate and bladder were studied through static models mostly for surgical training and rehearsal.

Synthetic kidney phantoms were developed by optimizing a mixture of gelatin and graphite powder to replicate both the elasticity and the acoustic properties of the natural organ (14), (18). In these cases, only the external anatomy was realistic but later works presented a biocompatible phantom kidney made from agarose gel that replicates some kidney critical structures (cortex, medulla, ureter and some lesions) (19) or the inner collecting system (pyelocaliceas system) (20).

For the puncture and drainage training in interventional urology and radiology, a gelatin-based kidney phantom that contains simple spherical cavities to represent the kidney calyxes was developed and validated as a valuable medical training platform. This phantom helps to practice coordination with both the surgical instruments and the US real-time images and improves the understanding of the surgical procedure and the most effective needle path. Indeed, the success of puncturing the target calyx is objectively assessed through visual evaluation of the fluid color drawn from the punctured area. However, the presence of marks left after the needle insertion is an unsolved issue that could be easily addressed by introducing novel soft and self-healing materials (21). While the hydrogels can be engineered to match some physical properties of the natural tissues, they usually have low tensile strength (20), resulting in fragile parts, see Figure 3. The introduction of silicone as base material allowed not

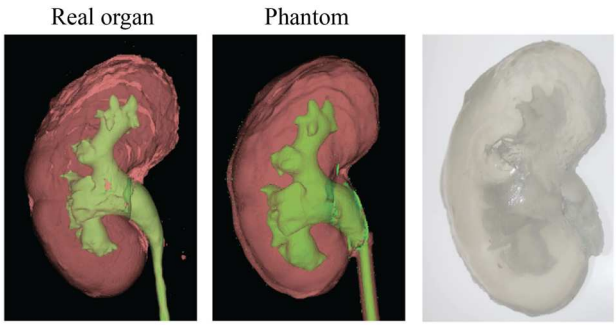

Figure 3 On the left, 3D reconstruction of the human kidney upon CT imaging data (real organ model and phantom model before printing), on the right a PDMS static phantom. Republished from (20).

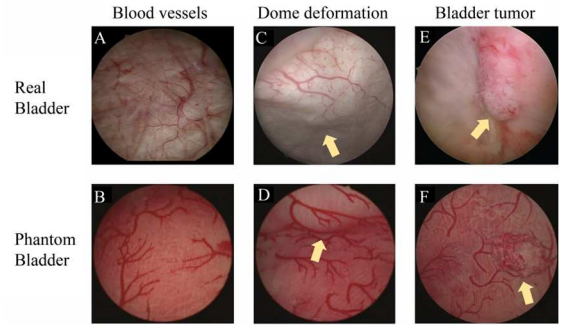

Figure 4 Bladder static phantom details compared with real bladder characteristics (blood vessels, dome deformation and tumors) during endoscopic training. Republished from (28).

only to increase the phantom durability but also the possibility of simulating the intrarenal hydraulic pressure, without the risk of phantom damaging (22).

Simple prostate phantoms were developed for the testing and validation of transrectal probes (23) and for the simulation of surgeries, such as the transperineal or transrectal needle-insertion procedure (24) or minimally invasive biopsy (25). In (24), the synthetic prostate was not anatomically correct, but the perineum, the rectum and the periprostatic surrounding area were created by using different polyvinyl chloride (PVC) mixtures to match the mechanical characteristics of natural tissues. The phantom deformation and haptic feedback were realistic upon needle insertion. Also, the phantom imaging under US, CT and MRI was comparable to *in vivo* data. An even wider study on the phantom materials selection was presented in (26), with the goal of mimicking not only the mechanical properties of natural tissues, but their thermal and electric conductivity. Two different compositions of PolyVinyl Alcohol (PVA), agar powder and hollow glass powder were selected to fabricate the peripheral and the central zones of the phantom prostate. The physical properties of this phantom enable a realistic simulation of the transurethral electrocautery resection procedure and a quantitative evaluation of the surgery through automated US image analysis. Also, the developed prostate phantom has realistic anatomic and haptic properties and thus it is suitable for the testing and validation of novel surgical instruments. Very recently, Gautam et al. described a PVA-based prostate phantom for use in US-guided prostate needle biopsy procedures (27). Although the external anatomy is correct and both the stiffness and the acoustic properties of the material are comparable to the human prostate, the internal morphology of the organ still needs to be replicated for an even more realistic phantom.

High-fidelity static urinary bladder phantoms were developed for cystoscopic training purposes (28), see Figure 4, as well as simulators of realistic imaging conditions (29), to evaluate novel optical coherence tomography systems and software for longitudinal bladder surveillance and early cancer detection (30). In all cases a relevant number of anatomical details was included in the design: from blood vessels to variable thicknesses and shapes. The high-fidelity phantoms were fabricated through molding techniques, in the first case with Ecoflex 00-20, while in the second with Poly(dimethilsiloxane) (PDMS) mixed with a 20:1 ratio between base and curing agent to increase elastic properties. The demonstrated simulators underlined how the realistic resemblance of materials, geometries and details result to be an extremely important factor towards the attainment of improved surgical skills.

Respiratory system

For what concerns the respiratory system, organs such as the trachea and the lungs were studied.

Indeed, as presented in (31), bronchoscopy simulation techniques, proved to be extremely useful in the process of learning in clinical practice. In the past years, multiple simulators both physical and virtual were studied, and some of them became also commercially available. However, novel physical simulators are still being developed for the replication of healthy and pathological tracheal tracts. In (32), authors developed a bronchoscopy simulator to train surgeons for retrieval of airway foreign bodies in children. Anatomical details were reproduced by 3D printing, with a digitally blended composite of rubber and plastic, an 18-months old child model acquired through CT imaging techniques. Surgeons evaluated the simulator by retrieving peanut fragments and 4 mm plastic beads. Although, there are some limitations due to the employed material properties that prevented from fully simulating a realistic condition, e.g. presence of saliva or tissue mobility, to improve the haptic feedback, the model successfully helped in the preprocedural training of surgeons. A similar approach was presented also in (33) where CT images of a pediatric laryngotracheal tract were employed to reproduce a model of a high-fidelity subglottic stenosis simulator. The phantom was casted in silicone within

a 3D-printed Polylactic acid (PLA) mold. The authors report the results of a Likert based survey: the surgeons felt that the phantom could be used for training with slight or no improvements, underlining once again the importance of a physical, low cost and portable model to guide the clinicians training or rehearsal and reduce negative surgical outcomes.

Different static lung and thorax phantoms were developed in the past years to study those cases where motion was not a fundamental performance parameter, e.g. to evaluate the effects of blast injuries (34,35) or radio therapies outcomes (36). In (34) the authors studied the properties of polyurethane foams to develop a surrogate lung material able to reproduce the real lung dynamic response, and to simulate the distribution of damage after blast impacts. To evaluate the extent of damage, Barium Sulfate-filled gelatin microcapsules with a diameter varying from 200 to 900 μm were mixed in the polyurethane foam with a ratio of 15:1 and tested through compression tests assessing mechanical properties. Capsule characteristics were evaluated both at low and high-rate impact speeds and different compression ratios. Stress speed waves were computed through the stress-strain relations while stress-time curves were used to obtain the hydrostatic pressure value for comparison with Bowen curves, which are commonly employed to predict the lethality due to free-field blast waves. Although the porosity was replicated using foam, the reproduction of the external anatomy was out of the scope of the work. The specimens resulted to have similar stress waves of lungs, as well as comparable bursting pressures of alveoli at injury, and similar extent of damage. Effects of injuries were also previously studied in (35), however in this case external anatomical details were taken into consideration. Indeed, a lung prototype based on average lung geometry CT images was fabricated by casted elastomeric urethane (Solid Concepts, Valencia, CA). The mechanical properties of the natural lung tissues were not replicated as the structure would not be otherwise able to sustain its own weight. The phantom was thus calibrated to understand whether it had adequate sensitivity and repeatability. The authors concluded that the device closely resembled a real patient lung in terms of spatial accuracy and was used to evaluate x-ray-based imaging quality and positional verification techniques for radiotherapy. The surrogate could estimate the impact velocity and energy; however, with continued testing also penetration depth may be estimated from the pressure traces. Internal and external anatomical details were reproduced in (37), where the thorax phantom was used to evaluate x-ray-based imaging quality and positional verification techniques for radiotherapy, and thus high fidelity was a fundamental requirement. The static phantom was fabricated through both casting and 3D printing techniques: a variety of materials were employed to provide similar kV projections of natural tissue. Gypsum for the bony structures (ZCorp zp151 high-performance powder, ρ=1.57 g/cm), Nylon (PA2200 Polyamide 12, ρ of laser sintered part = 0.93 g/cm^3, bulk ρ=0.45 g/cm^3) was used for the airways, lung blood vessels, outer lung surface, and tumors and was printed using Selective Laser Sintering (SLS) (distance between laser lines = 0.25 mm, one laser line = 0.4 mm, layer thickness 0.1 mm, EOS GmbH, Krailling, Germany). Silicone (Dragon Skin 30, Smooth-On Inc., ρ=1.08 g/cm^3) was used for the soft tissue (mediastinum, muscles, fat, skin) and was cast into the mold of the body contour that was 3D-printed using SLS. All 3D-printed components were manually assembled and glued to a Poly(methyl methacrylate) PMMA build plate using a hot melt adhesive after which the silicone was cast into the mold of the body contour. The authors were able to develop and test an anthropomorphic phantom, that with its life-like features and radiation hardness was made useful for optimization and validation of image acquisition, processing, reconstruction, and registration algorithms. The manufacturing process is still the most challenging part of the development as correct alignment and positioning are difficult to be obtained.

Cardiovascular system

Within the cardiovascular systems, organs as the heart, valves and vessels were studied mostly to guide medical training procedures. Soft robotics materials and technologies became of paramount importance also within this field to obtain realistic simulators and improve surgical skills outside the operating room.

Passive and static simulators of the heart were developed for the medical training of specific procedures, such as transseptal puncturing (38), US-guided pericardiocentesis (39) and epicardial hydrogel-sheet placement (40). Studies on the employed materials for the heart phantom manufacture were conducted to increase the realism of its appearance under US (41), and to mimic both the mechanical (42) and electric properties (43) of the heart tissue.

Some cardiovascular diseases affect the heart valves shape, mechanical properties and thus functionalities. The pre-operative availability of low cost, patient-specific static models, are therefore of incredible help to the surgeons both while studying a case and for pre-surgical rehearsal. Generally, after acquiring images through transthoracic echocardiography (TTE), (44), or trans-esophageal echocardiography (TEE) combined with CT (45), 3D models of mitral valves were built. These models were then fabricated through 3D printing techniques (44,45), and sometimes also molded to be compared with the printed versions, as in (44). In the latter case, TangoPlus PLX 930 (Stratasys Ltd.) Shore A 26-28 was compared to a molded phantom in Dragon Skin Fast and Medium (Smooth-On Inc.): reported results show that molded valves were able to better simulate the natural tissues with a lower cost with respect to the 3D-printed ones. However, in future, improvements in additive manufacturing techniques and materials could overcome these limitations.

Authors in (45) worked instead on a multi-layered structure fabricated with different Shore A hardness of TangoPlus from 27 for mitral leaflet outer shell and surrounding tissue, 35 for the inner layer, to 60 for the papillary muscle. Pathological deposits were instead 3D-printed with VeroWhite material (Stratasys Ltd.). Although the 3D modelling limitations, the produced mitral valve was sufficiently realistic to understand pre-operative challenges and simulate catheter-based mitral leaflet repair procedures.

Vessels are static organs responsible of carrying the blood within the body. Phantoms were developed to test through imaging techniques patient-specific static and/or dynamic conditions (46–49) or to simulate preoperatively transcatheter aortic valve replacements (50–55). or again to optimize CT techniques (56).

In the first case, if a vascular network phantom was developed, usually a 3D-printed patient-specific mold was fabricated and a polymeric material with the desired mechanical properties was casted (with dip or brush coating techniques). In (46) authors compared different candidate materials both in terms of mechanical properties and imaging appearance (e.g. polyurethane rubber (Brush-On 40, Smooth-On Inc.), platinum-cured silicone rubber (Ecoflex 00-35), platin-cured silicone rubber (Moldmax 10 T, Smooth-On Inc.), and latex rubber (Moldcraft FMF, Burma Rubber Co.). In (47), instead, a number of latex layers were chosen to fabricate the system, and successively tested in an *in vitro* flow mock-loop setup. In some cases, casting techniques were compared to 3D printing to understand the usability of vascular phantoms for imaging purposes (49). In (48), instead, authors developed a model of a severe patient-specific aortic stenosis condition. In this case, the presence of tissues (i.e. calcific regions and soft tissues) was replicated through the introduction of different 3D-printed materials. The phantom was then tested in dynamic conditions and evaluated through imaging techniques, with the purpose of developing patient-specific treatment strategies.

As in (54), 3D printing of rubber-like materials has been frequently employed also for the development of models for preoperative planning. The design of printing parameters (49), and/or materials (51) was, thus, fundamental to obtain the desired mechanical properties.

To mimic the complex aortic mechanical properties, different studies also focused on the development of patterned structures, manufactured with 3D printing techniques and sometimes combining them to casting. In (50), for example, the authors compared Agilus–VeroCyan (Stratasys Ltd.) specimens to Dragon Skin 30–TPU 95A ones, where the first two materials served as base, while the others were employed to 3D-print five different patterns. The Dragon Skin 30–TPU 95A specimen met the criteria set for strain at breaking but had insufficient tensile strength. The Agilus–VeroCyan specimens, instead, demonstrated lower strain at break than the Dragon Skin 30–TPU 95A specimens for all the patterns. To test the composites more precisely, however, a tubular pattern would be needed, combined possibly with a new testing method. In (53) the authors 3D-printed different helical patterns within a base material to replicate the function of collagen within the aortic tissue. Successively the same method was used to manufacture an artificial tissue-mimicking and patient-specific aortic wall specimen (52). After deploying the CoreValve, the entire system was studied to quantitatively predict a possible paravalvular leak in case of transcatheter aortic valve replacement.

2. Dynamic synthetic simulators

2.1. Passive simulators

Dynamic passive simulators enabled the study of particular organs under specific working conditions, thanks to the introduction of external actuation methods.

Figure 5 Dynamic simulator of human larynx. Courtesy of Dr. Martina Maselli, Scuola Superiore Sant'Anna, Italy.

Sensory organs

Starting from the sensory organs, the eye was studied because of its self-regulation: this ability is indeed enabled by its autofocusing motion and its large dynamic range, which make it the ultimate "imaging device" and a continuous source of inspiration in science. In (57) a liquid crystal elastomer iris was described, which can autonomously open and close by responding to the incident light intensity, without any need for external control circuitry. Similar to natural iris, the device closes under increasing light intensity, and upon reaching the minimum pupil size, reduces the light transmission by a factor of seven.

Respiratory system

Within the respiratory system organs as the larynx and the lungs were studied.

Larynx simulators are useful platforms for clinical investigations that help clinicians understand the pathophysiology of vocal folds in general. Among the different categories of larynx simulators, the synthetic model

represents the most appropriate one, able to replicate its main components and functions. Self-oscillating synthetic models (58–65) are based on elastomeric material with viscoelastic properties similar to the biological tissue and properly designed to achieve advanced and more-realistic self-sustained, flow-induced vibrations at characteristic frequencies comparable to those found in the human vocal folds. They generally rely on one (60,61) two (62,63) or multi-layered (58,59,64) (Figure 5 (59)) approaches and are relatively easy to manufacture. A different approach using a 3D printing technique based on embedding a UV-curable liquid silicone into a gel-like medium was developed and demonstrated in (65), in order to reduce model fabrication time and increase yield. The advent of dynamic vocal folds modeling attracted researchers' attention because of the capability of replicating self-sustained oscillations close to the biological system, by using silicones with specific mechanical properties. The self-oscillating models are useful in voice research, e.g., in evaluating collision force between the vocal folds, in assessing supraglottal aerodynamics and in developing *in vivo* measuring devices.

Synthetic dynamic passive lung phantoms were instead developed to tackle some of the biggest clinical challenges related to the respiratory motion. These challenges are related to the correct synchronization of the breathing pattern of each patient to the acquisition of clear CT images or the accurate administration of radiation therapies, in case of tumors. In these situations, the presence of deformable dynamic phantoms is crucial. The so far developed phantoms, usually, focus on the replication of the imaging properties of the lungs, while the motion is implemented by an external motor connected to a shaft and a rigid or soft plate pushing the artificial lungs, replicating the natural action of the diaphragm (46,66–72). Just a few, implementations instead maintained an anthropomorphic shape, and a pneumatic actuation (36).

Studies in the early 2000's, mostly neglected the anatomical details, building systems of cylindrical shape and motor-driven (70–72). This trend was continued also by the work presented in (66): here, the authors used a water-immersed sponge, placed in latex balloon to simulate the imaging properties of the lungs. The tumors were instead reproduced as water balloons, or silicone or glass balls. To mimic the presence of other organs and structures the cylinder containing the artificial lung was filled with water, and a silicone membrane replicated the action of the diaphragm.

Although the early versions of the device served for calibration activities, successive versions were employed to analyze dose differences during respiratory motion (67). In this case, tumors were casted with silicone rubber (Liquid silicone RTV-S3, Korea), and the diaphragm was replicated by an acrylic plate. The motion data was then acquired through Four-Dimensional Computed Tomography (4DTC) imaging. The phantom could be used to quantitatively analyze the dosimetric impact of the respiratory motion according to the factors that influence the difference between the 3D and 4D dose, such as the tumor size and motion.

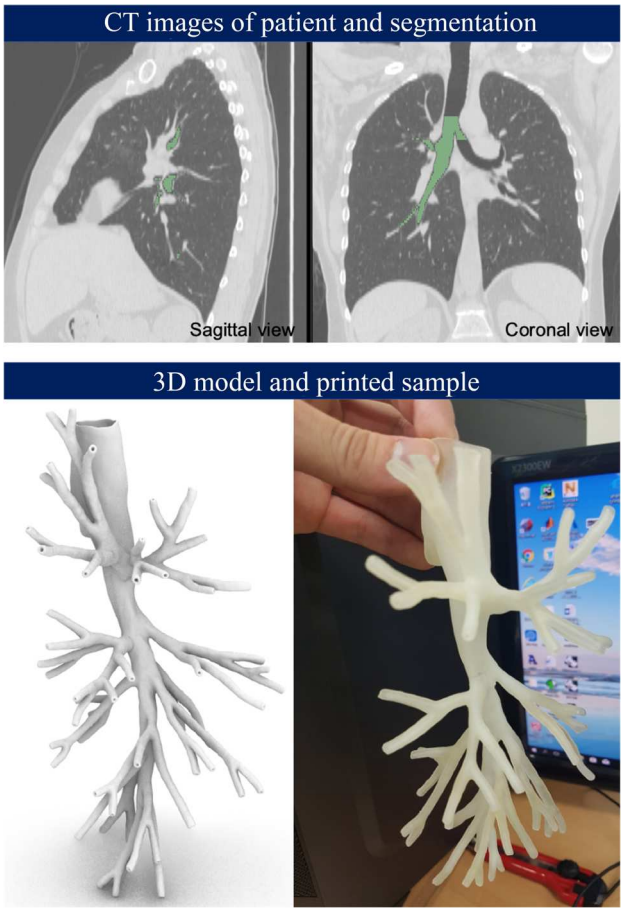

Figure 6 CT imaging based passive simulator of the human lungs. On top an example of the acquired images, at the bottom a simplified CAD model and the 3D printed sample. Courtesy of Dr. Dong-Seok Shin, and Prof. Tokihiro Yamamoto, Department of Radiation Oncology, University of California Davis, USA.

The device was further improved to take an additional step towards complete deformability and anthropomorphic appearance (66): 3D-printed flexible airways were manufactured with TangoPlus rubber like material and successively casted FlexFoam-IT V (Smooth-On Inc.)., polyurethane foam, see Figure 6. The airways model was obtained on the basis on the available breath-hold CT data of a human lung: the reproducibility of the phantom was thus evaluated during artificial breathing cycles.

The importance of a fully anthropomorphic appearance of the phantom was introduced in the work of Mayer et al. (68), where a dynamic, yet passive phantom was developed using 3D printing manufacturing techniques, taking into consideration Hounsfield values of the employed materials. The thorax was manufactured in such a way it could emulate soft tissue and bone properties: Tango Plus (83 HU) for the soft tissue and Vero White (136 HU) for the bone; the lungs

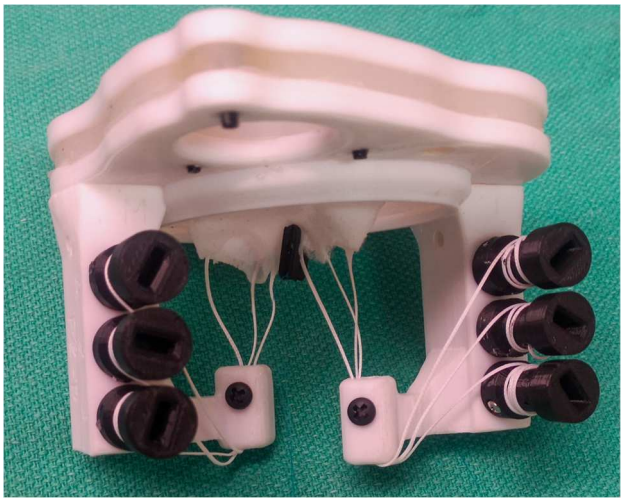

Figure 7 Passive simulator of the human mitral valve. Courtesy of Dr. John Moore and Prof. Terry Peters, Robarts Research Institute Western University, Canada.

were mimicked instead through wet sawdust, as it resembled more closely the patient HU values.

Perrin et al. (36), also, built and anthropomorphic phantom, comprising other organs, as well as bony structures and skin: the realism was important feature as in pencil beam scanning proton therapy in the thorax both motion of intervening tissues (ribs) and motion of the target are critical, and produce degradation in the target dose distribution.

The lungs were manufactured using a polyurethane foam (EZ DRI Supersoft, Crest Foam Ind., NY, USA) coated with PU spray deposition (SEETHAN 4709, See-Plastik GmbH, Seeshaupt, Germany) in order to obtain an air-tight 0.3-0.6 mm thick coating. The diaphragm was, instead, constructed out of a latex cloth (Suter Kunststoffe, Fraubrunnen, CH), which, due to a higher material elasticity, allowed for large target motion. A tumor was positioned within the lungs and its motion was studied. Different typologies of tumors were manufactured: two were constructed from wooden spheres of 30 and 60 mm of diameter sliced into 1 cm thick disks for sandwiching of radiochromic film, while for easier visualization in MRI, an alternative spherical silicone tumor (60 mm in diameter) was also modelled (Plastic Gel 10, Fritz Minke, Germany). The phantom was pressurized following user-defined breathing patterns, allowing the test of both regular and irregular breathing patterns from simulated or real sources. Three imaging and tracking modalities have been tested using the phantom: 4DCT, MRI and the Calypso RF-transponder motion tracking system. The main limitation encountered was the time-consuming nature of film dosimetry in this phantom, due to the large number of variables to be explored, and thus the authors suggested the future possibility to include a remotely resettable dosimeter. Despite this consideration, the device presented convincing capabilities for being utilized to test new devices like 4DCT, surface imaging, Four-Dimensional Magnetic Resonance Imaging (4DMRI) and gating, needed for the treatment of moving tumors. An anthropomorphic shape and realistic breathing patterns were presented in (73), where a dynamic passive phantom was developed for positron emission therapy, the most widely used tumor detection technique. The performed tests, validate the performances of the phantom, obtained by filling with foam a case obtained by CT imaging.

Digestive system

Dynamic passive systems were developed also to study specific conditions of the gastrointestinal tract. One of the commercially available devices, named Mikoto, is for example, able through an electromechanical system to simulate different abdominal pressures or the reposition due to deep inspiration, as well as to provide feedbacks during the training session (74). Another solution was also presented in (75), where a modular casted intestine was presented. The system was fabricated with an extra-soft silicone (Ecoflex 00-30) and made airtight. The device can be repositioned through an electromechanical system, but it also presents the possibility of replicating the peristaltic motion of a specific portion, thanks to a pneumatic sleeve, sequentially activated.

Cardiovascular system

Within the cardiovascular system, dynamic versions of valve phantoms were developed in order to simulate pre-operatively mitral and tricuspid repair outcomes. The first version (76) of a patient-specific model was developed based on TTE mitral valve images collected from 10 subjects, successively transformed into 3D models through the 3D Slicer software. The 3D models were then translated into a mold, and a tissue-mimicking silicone was casted (Ecoflex 00-30) reinforced by gauze fabric, to create realistic suturable leaflet material. Chordae were replicated, with braided nylon thread (77), see Figure 7. The models were then inserted in a heart phantom simulator, and the behavior was compared with patient-specific data, before and after mitral valve repair. The same workflow was then presented in the case of tricuspid valve pre-operative simulation and planning (78). In this case TTE images were employed. The results, however, indicated that still some manufacturing issues should be addressed to improve the models, as neither TEE nor TTE images could consistently capture the leaflet or papillary attachment points of the chordae tendineae, forcing the authors to estimate these locations, and thus impacting on the final results. Although preliminary, this study showed the potentiality of the presented workflow to practice valve repair preoperatively, shedding the light towards the simulation of complex anatomical pathologies that could not be otherwise closely observed.

2.2. Active simulators

Many research efforts were dedicated to the development of synthetic simulators of those human organs that are characterized by a motility, such as the peristaltic contractions of the gastro-intestinal tract, the respiratory motion of the diaphragm and the lungs or the heart pumping.

Sensory organs

While most of the synthetic organ simulators were used as platforms for the medical training and the testing of new medical devices, active facial skins able to reproduce human-like facial expressions were introduced in humanoid soft robots not only to improve the non-verbal communication with humans, but also to enable their interaction with the environment, through a soft skin that can sense touch and proximity (79). To replicate human facial expressions and emotions, the skull of a humanoid robot can be covered by a soft and actuated elastomeric skin that is pulled from specific control points and directions. The distributed actuators should be small and compact to be integrated in the skull of the robot, easy to be finely controlled and have short response times, in the range of few milliseconds. Different actuation strategies were explored in literature. The humanoid robot that demonstrated of being able of basic face movements (opening and closing of the eyes, smiling) had a cable-driven skin whose cables were pulled by a piezoelectric motor (80). The miniaturized motor allowed high resolution in displacement, fast response, and high force per unit area, but the motor is still an additional rigid element. The robot Mark I integrated rigid air cylinder type actuators and both the dimensions and weight of the robotic head were excessive with respect to a human head (15 kg and 1.5 times larger) (81). Later, the upgraded version Mark11 had a silicone face skin moved by miniaturized Shape Memory Alloys (SMAs), that were electrically driven. The robot generated six typical human facial expressions (surprise, fear, disgust, anger, sadness, and happiness) through a SMA arrangement that was inspired from the anatomy of human facial muscles and their directions of contraction. The employed SMA actuators satisfied the application requirements of displacement and force, contracted quickly (1 s) but needed 8 s to recover. A forced cooling through a small fan was introduced to get round the problem, getting a 2 s recovery time, but the contraction phase was slowed down too. In addition, it was challenging to geometrically arrange all the components in the skull, also positioning the SMA actuators without touching each other's (82). To overcome these limitations, in later versions of this robot, the McKibben actuators were selected (83). The similarity of McKibben actuators to muscular fibers and the bioinspired disposition (84) underneath the elastomeric skin of the robot face allowed a realistic simulation of six facial expressions which resulted easy to be recognized by human beings (85), see also Figure 8. The introduction of flexible pneumatic actuators, such as McKibben actuators, increased not only the robot biomimetics but also the overall robot safety and acceptability, promoting a tighter human-robot interaction (79).

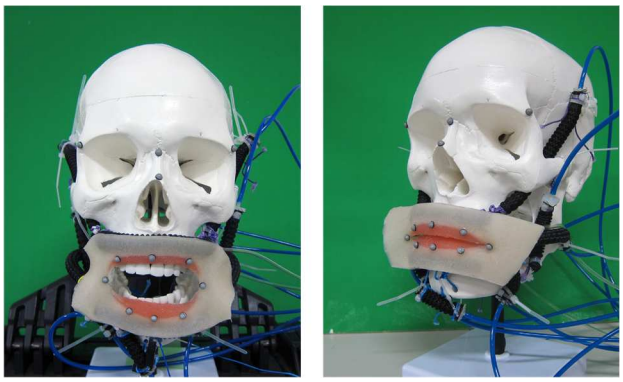

Figure 8 Face robot having a soft mouth with embedded soft artificial facial muscles, capable of generating facial expressions. Courtesy of Dr. Ryuma Niiyama, University of Tokyo.

For the robot communication based on optical principles, but also in several other fields of application, such as consumer electronics and medical diagnostics, optical lenses with tunable focus characteristics are desirable. To address this need, lenses made of smart materials able to respond to mechanical, magnetic, optical, thermal, chemical, electrical, or electrochemical stimuli are intensively studied. In (86) the potential of a different class of 'smart' materials to develop electrically tunable optical lenses with simple and compact structure, low weight, high response speed, and low power consumption are shown. The optical device is inspired by the architecture of the crystalline lens and ciliary muscle of the human eye. It consists of a fluid-filled elastomeric lens integrated with an annular elastomeric actuator working as an artificial muscle. Pieroni et al., described a configuration to obtain compact electrically tunable lenses entirely made of soft solid matter (elastomers) (87). This was achieved by combining the advantages of the Dielectric Elastomer Actuation (DEA) technology with a design inspired by the accommodation mechanism of reptiles and birds. Whereas, in (88) the deformation of the tunable soft lens is achieved by the actuation of DEAs, mimicking the change of the surface profile of the human eye to achieve remarkable focal length variations. All these studies are of paramount importance since tunable lens technology inspired by the human eye has opened a new paradigm of smart optical devices for a variety of applications due to unique characteristics such as lightweight, low cost, and ease of fabrication over conventional lens assemblies.

Digestive system

For what concerns the digestive system, several dynamic simulators were developed to replicate the anatomy and the

Figure 9 Swall-E system. Courtesy of Yo Fuijso (INSERM UMR-S 1121 'Biomaterials and Bioengineering', Strasbourg University), Pierre Mahoudeau (ENT Department, Strasbourg University Hospital) and Christian Debry (ENT Department, Strasbourg University Hospital and INSERM UMR-S 1121 'Biomaterials and Bioengineering', Strasbourg University).

movement of structures such as the tongue, the esophagus and the stomach.

Test set up and simulators that can reproduce the physiological movements during swallowing and digestion, and concurrently measure parameters of interest, such as the force applied by the tongue on the (89,90) are of particular importance to give a mechanistic explanation to some *in vivo* observations (91) and also for the development of treatments for patients with disfunctions related to the digestive process, such as dysphagia (92). The Cambridge Throat is a mechanical system in which the bolus dynamics matches *in vivo* data (93). A flat and deformable polyethylene membrane was attached to a rigid structure that represents the upper throat and the pharynx. The bolus propulsion induced by the tongue was simulated by a rigid roller that, attached to a revolving shaft, was moved by a set of hanging weights (94). However, a realistic representation of the tongue is desirable (95), considered the fundamental role that the tongue shape and movement have during swallowing. The dynamic video fluorographic swallowing study simulation system reproduces the human anatomy of the tongue, the pharynx, and the larynx. A wire-driven mechanism constituted by sixteen DC motors deforms the synthetic silicone conduct. The inextensible wires were positioned around the conduit to mimic the action of the human muscles involved in the pharyngeal swallowing process. In particular, the tongue position was controlled by two wires connected to the hyoid bone, while the tongue shape was determined by three additional wires, connected to the tongue center point and tip (96). The cable-driven actuation strategy was implemented in the Swall-E simulator (97), Figure 9, and very recently in a robotic tongue showing contraction and bending capabilities (98). Swall-E is a complex and robust system with high spatial (0.025 mm) and temporal (20 ms) resolution. In addition to the movement of the base of the tongue, it also reproduces important physiological mechanisms occurring during the pharyngeal swallowing, such as the epiglottis tilt, the laryngeal elevation and the vocal folds opening and closure. In addition, it is designed to simulate a respiratory air flow, to also study the interaction between the respiration and the swallowing dynamics. For the simulation of the tongue movement and interaction with the surrounding anatomical structures, a pneumatic actuation was also explored. A soft robotic tongue made from three layers of patterned silicone to create inflatable chambers (99) was controlled by an optimized electrical and pneumatic circuit to achieve typical tongue motions, such as roll-up, roll-down, elongation, groove, and twist. In (100), a robotic tongue made by casting silicone was deformed by applying both positive pressure and vacuum to the inner pneumatic chambers. The tongue is inserted in a rigid and sensorized system that simulates the oral cavity and measures both the palatal pressure exerted by the soft robotic tongue and the bolus velocity, through an ultrasound probe. A key limitation of the described models is the unphysiological tongue and palate surface texture, and the lack of saliva lubrication (90). Besides some models replicate the wettability of the tissue, such as the contact angle between saliva and tongue surface of approximately 50 deg (100), the realism of the swallowing simulation would be further increased by the introduction of lubricating films that have the rheological and tribological properties of the human saliva. Very recently, the concept of a pneumatic tongue based on inflatable and connected chamber was further explored in (101) designing up to 32 chambers. In (102), the pneumatic actuation was combined with SMAs to achieve not only tongue elongation and contraction, but also curling, and demonstrating the capability of grasping objects and liquids with a maximum volume of 13 ml.

In the swallowing process, the bolus is displaced from the mouth to the stomach through the peristaltic action of the muscular bundles constituting the esophagus. Any esophageal impairment that leads to ineffective swallowing is known as dysphagia: it can be caused, for instance, by benign

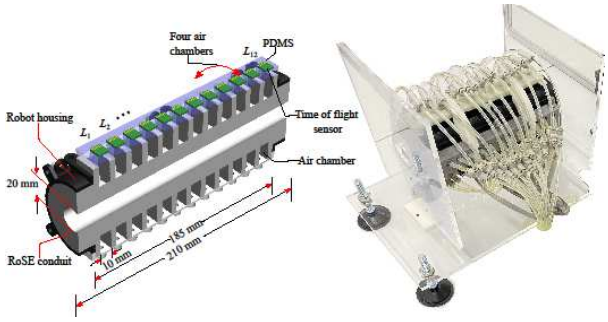

Figure 10 The RoSE system, a biomimicking soft robotic esophagus, developed for testing in vitro endoprosthetic stents for dysphagia management. Courtesy of Dr. Dipankar Bhattacharya and Prof. Peter Xu, University of Auckland, New Zealand.

esophageal strictures from various injuries, esophageal cancer, esophageal perforations, or distressing lumen patency. Depending on the severity, different solutions are available from nasopharyngeal feeding tubes to surgical corrections and esophageal stenting. Understanding the pumping motion of this organ is of valuable importance, to develop alternative solutions or test the present ones before implantation.

Different esophageal simulators tried to replicate the peristaltic motion of the organ. Although, the employed technologies were mostly pneumatic (103–107), (108) and (109–111), a similar motion was also implemented through cable-driven technologies, as it is in the case of Swall-E (97) or through magnetic technologies (97).

The Robotic Soft Esophagus system, i.e. RoSE, is a pneumatic device able to replicate the peristaltic motion of the organ by coupling the activation of inflatable rings in sequence (103). Each ring (104) is composed of 4 pneumatic chambers, positioned around a cylindrical tube: they able to inflate radially restricting the canal upon pressurization. The actuator is reinforced externally by an Acrilonitrile butadiene styrene (ABS) casing to avoid outward expansion, while enhancing the inward one. The body of the actuator was manufactured through lost-wax casting techniques with Ecoflex 00-30, eventual connections were sealed instead with Sil-Poxy glue (Smooth-On Inc.). The luminal conduit is of 18 mm internal diameter has a thickness of 8 mm, the chambers are 10 mm in height and are discretized by 5 mm of silicone rubber, in total 12 actuated rings compose the overall system, its characterization is presented in (106). Further modelling improvements and insights on the single ring-shaped actuator were presented in (107). The RoSE system, see Figure 10, was also tested for synthetic bolus swallowing and as pre-clinical simulator before stent implantation (105), however future studies will investigate the interaction with artificial saliva and embed a stretchable sensor to close the control loop and measure radial pressure and conduit strain. Based on the same design, Ruiz-Huerta et al. (112), recently presented a study aiming at the X-ray visualization of the bolus flow through the esophageal tract, to understand the system dynamics during the swallowing action. The work confirmed the presence of extensional flow as the bolus is stretched and compressed during peristalsis.

A similar design approach was presented by Esser et al. (109) for pumping applications. Initial versions of this peristaltic pumping device were fabricated with inflatable 8 foam rings (FlexFoam-it VI and X, Smooth-On Inc.) reinforced with polypropylene tape. The study reported a 50% radial contraction at 0.8 bar at 0.4 Hz, while at a pressure of 1 bar and frequencies of 0.5 to 0.55 Hz contractions in the range of 60% could be achieved. However, to overcome durability issues, a silicone-based version (Ecoflex 00-50) was presented in (110), with an elliptical lumen to improve radial contraction ratios. For this reason, occlusion rates up to 99.8% were achieved as well as 15,000 cycles were sustained instead of the previous 500. Finally, the biomimetic device (111) was tested to evaluate flow characteristics and efficiency of pumping, although the scope of the work was not to use the device as simulator, the achievements could be of great help in any case to the biomedical field.

The same applies to the work of Li et al. (108), where the swallowing was replicated through a fluidic robot, guided through a compliant tubular structure. The structure is a double-layered capsule, made of silicone rubber. The motion, however, in this case, is guided through a linear traction body. The device was tested to measure the pull-off force both with air and water as driving media.

The esophageal peristaltic motion was replicated also with different actuation technologies. Good performances were obtained with a magnetically actuated silicone tube, embedding metal particles (110). The tubes were fabricated with PDMS mixed with metal particles from 50 to 75WT% metal particles, both with circular and elliptical tubes. The presence of the metal particles allows lumen striction when magnetic field is present.

The cable-driven Swall-E system (97) simulated a healthy peristaltic esophageal motion with synthetic bolus based on *in vivo* timings reported in normal swallowing studies. The clinically relevant data that are obtained could reduce the number of animal experiments, as well as the discomfort of patients with swallowing disorders.

For the simulation of the food digestion process in the stomach, dynamic models such as the Gastric Digestion Simulator (GDS) (113) and the Human Gastric Simulator (HGS) (114) were developed. The biochemical processes are represented but neither the stomach anatomy nor motility is realistic (115). Indeed, the compliant and constantly moving nature of the organ makes the shape definition challenging. Real imaging data of different digestive phases obtained through computer tomography gastroscopy are needed for a morphological representation of the organ as close as possible to reality (116). An anatomically accurate stomach simulator

made from silicone was developed for the validation and testing of surgical robotic devices (117). The model can deform and contract through a cable-driven system constituted of four miniature wires positioned around the outer surface of the stomach phantom, but the simulated motion is poorly realistic. The mechanical peristalsis of the human stomach is the Antral Contraction Wave (ACW), a cyclic decrease in the diameter of the organ (118). SoGut is a unique soft robotic gastric simulator able to simulate the ACW through the sequential activation of modular ring-shaped pneumatic actuators that radially contract, covering the required average amplitude of displacement and force that characterize the human stomach contractions (119). Preliminary studies focused on the actuator design and theoretical modelling (120) (119). A custom-made soft sensor was integrated into the inner surface of the actuator without affecting the actuator compliance (121). The sensor is an elastomer filled with electrically conductive carbon particles; the electrical resistance variation of the sensor was related to the radial deformation of the actuator, enabling closed-loop control. Also, a model-enhanced control scheme for precise control on the contraction of a ring-shaped pneumatic actuator is described in (122). In the SoGut platform, the inflation sequence of the ring-shaped actuators can be coordinated in time and space to simulate both healthy and diseased gastric motility in a repeatable and quantitative manner. However, the limited number of actuated modules restricts the contraction at discrete points. In future developments, the smoothness of the ACW can be improved by increasing the number of actuators (123). Very recently, a bellow-driven soft pneumatic actuator with self-sensing capabilities was designed to replicate smooth muscle contraction in the gastro-intestinal tract (124). The occlusion ratio of a human stomach antrum and the peristaltic waves were simulated with a single module (125). However, the development of a complex stomach simulator that mimics natural movements by integrating several actuation modules is a future challenge (126).

For what concerns the synthetic sphincters, the physical simulators that incorporate the anal sphincter tone and replicate the haptic feelings are highly beneficial to learn the medical skills needed in the digital rectal examination, a physical exam for the first inspection of colorectal and prostate abnormalities. In (127), an anal sphincter simulator whose tone was motor-controlled by pulling and releasing cables wrapped around a silicone model is presented. The significant friction between cables and silicone, and the non-uniform application of force around the opening, highlighted the intrinsic limitations of the cable-driven simulator, with respect to a more realistic pneumatic model (128). Indeed, the action of the two natural muscles that are symmetrically wrapped around the anus was replicated by two independently actuated pneumatic chambers, integrated in a multi-layered sphincter model made of different stiffnesses silicone rubbers. The pneumatic actuation and the use of soft materials gave an optimal haptic perception, that was evaluated in a user study with ten colorectal expert practitioners on reaction time, pressure level, pressure quality and similarity to a real case. The described sphincter model replicates the pressure profiles of real patients, that were obtained from the anorectal manometry exam. Future developments of the pneumatic driving circuit will also allow the simulation of fast dynamics (129), such as the fast movements associated with the natural cough reflex.

Respiratory system

Moving the attention to the respiratory system, soft robotic diaphragm and lungs simulators were studied. The human respiration is the result of a complex mechanical interaction between the diaphragm, lungs, pleural space and abdomen. The diaphragm is the biological structure that, moving downward, decreases the pleural pressure to below the pressure at the airway opening, thus driving the airflow into the lungs. Simultaneously, the abdominal pressure is increased. From a clinical perspective, the pleural and abdominal pressures are the most important output parameters during respiration (130), but volume changes are also significant (131) and lead to internal organs movements. Interventional radiologists recognize that the motion during respiration is a challenge for the targeting of a lesion during diagnosis and radiation therapy (132). Deformable image registration algorithms are used in adaptive radiation therapy, and dynamic physical simulators with different complexity have been developed for their evaluation and validation. A belt with inflatable air bags, commonly used for the blood pressure measurement, was tied around a dummy torso in which anatomically accurate organs made from different gel mixtures were accommodated (132). This simple mechanical apparatus could produce deformations in the superior-inferior (SI) direction only, with limited controllability, while the internal organ deformation during respiration is complex and multidirectional forces are needed. The respiratory motion is also recognized as the main cause of misdiagnosis and insufficient treatment of needle-based interventions for liver cancer, the second leading cause of death worldwide (133). In (134), a synthetic liver is positioned on a rigid plate moved by 3D-printed bellow-shaped soft pneumatic actuators both in the SI and anterior-posterior (AP) direction. Different respiratory patterns with variable breathing depths and speeds were replicated with acceptable accuracy and repeatability, but the liver deformations that arise from the interaction with the surrounding natural tissues and organs is not represented. The diaphragmatic movement was also replicated by applying pressure to a phantom torso constrained between a fixed and a translating rigid plate, that was displaced by a mechanical piston (135) or a stepper motor. However, there is a mismatch between the mechanical characteristics of the homogeneous

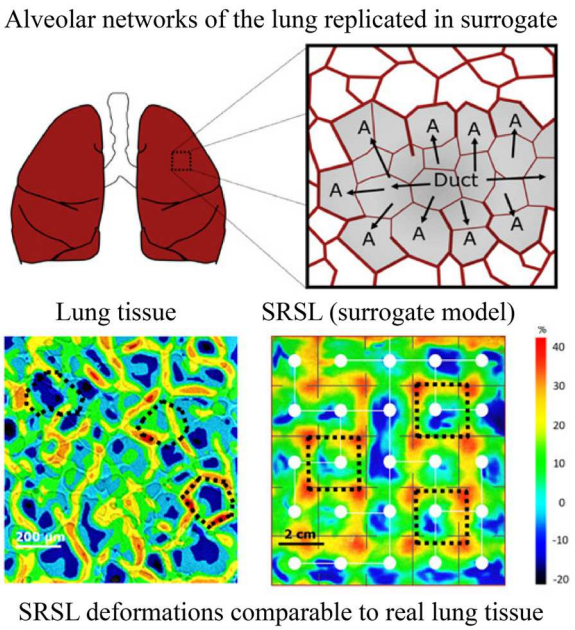

Figure 11 Soft surrogate lung developed to predict injury risk upon traumatic events. The image shows the comparability of results in terms of deformation between natural lung tissue and the surrogate model. Republished from (139).

liver-supporting soft material and the natural abdomen (136). In addition, at the interface with the rigid plates, larger liver deformations were observed if compared to *in vivo* data from 4DCT (137). Very recently, the function and motion of the natural diaphragm were recreated by introducing various soft robotics technologies. A respiratory simulator constituted by an active soft robotic diaphragm was presented in (138). The phantom can reproduce the patient-specific breathing motion when synchronized to real-time data acquired from a sensorized belt worn by the patient, but the simulator actuation, material, and multiscale structure could be improved. The active diaphragm structural complexity was increased in (133) by combining vacuum-actuated soft actuators with bending and contracting pneumatic actuators and elastic wires. In this MRI-compatible soft robotic platform, the diaphragm displaces in both SI and AP directions a synthetic liver, but the simulated motion pattern deviated from the modeled one at fast respiration speeds. At present, the accurate simulation of the diaphragmatic motion during respiration with a soft robotic diaphragm, also accounting for the interaction with the abdominal organs and tissues is still an open challenge. In (130), a high-fidelity anthropomorphic model that combines advanced robotics and organic tissue is presented. The anatomically accurate diaphragm made from elastomeric and thermoplastic materials is connected to several McKibben actuators that, when activated, recreate the pressure changes that cause the organic lungs to inflate and deflate, during both regular breathing and diseased states. This benchtop model, being anatomically and physiologically accurate, represents a vast improvement over previous models and can be used not only as a relevant testbed for novel devices, but also as a research tool to elucidate fundamental physiological concepts of human respiration. Additional advances could be made by further increasing the diaphragm biomimicry, by developing an actively contracting artificial diaphragm whose mechanical properties, such as stiffness and thickness, could be independently varied to replicate pathologic changes too. In addition, the replacement of organic lungs with robotic lungs would be highly desirable, to avoid the complex management of natural tissues and strongly improve the usability and durability of the respiratory simulator. In 2019, a soft robotic surrogate lung was developed by Ranunkel et al. (139), see Figure 11. The authors worked on the replication of clusters of artificial alveoli, able to mimic their dynamic basic movement, to understand the damaging nature of local defects caused by occlusion or overdistension. The alveolar structure presented was simplified to a 5x5 network of cubic elements, casted with silicone rubber. The elastomeric material was chosen by comparing Ecoflex 00-10, Ecoflex 00-30, Dragon Skin 30 and 50 to elastin and collagen mechanical properties, and finally Ecoflex 00-30 was selected as falling in the correct stress-strain range. The device was tested in pressure-volume measurements, to assess the ventilation behavior, i.e. lung compliance, and strain measurements were used to study pathological conditions. Finally, blast injury studies to both biological and nonbiological samples were performed. Despite some limitations in terms of geometrical complexity and fabrication techniques, the results show encouraging data, that could bring to the future development of a surrogate lung model accelerating the progress of therapeutic and preventive interventions for lung diseases.

Cardiovascular system

For what concerns the cardiovascular system, many research efforts were dedicated towards the development of cardiac simulators for various purposes, such as medical training and cardiovascular devices testing and validation. Dynamic heart simulators were developed for the validation and optimization of different cardiac imaging techniques, such as myocardial scintigraphy (140), US (141,142) and dynamic single photon emission computerized tomography (143). These simulators create a cardiac-like beating motion by cyclically varying the pressure inside the ventricular cavities, and no soft actuators are employed. In (144), a left ventricle phantom made by casting PVA is described. A pulsatile hydraulic pump inflates and deflates the ventricle that simulates the apical twist observed in the natural heart through the arrangement of two PVA layers with different elastic properties in a spiral pattern. This twisting ventricle simulator can cover the twisting range of normal and ischemic hearts, but not all peak values that are clinically reported. Indeed, in

the natural heart, the peak systolic twist value is determined from the clockwise rotation of the heart base and the counterclockwise rotation of the apex, a deformation that is challenging to be mimicked in a physical simulator (144). To realize simulators for the medical training on a beating heart, cable-driven (145) and cam-follower mechanisms (146) were introduced. In (147) and (148), the PVA-based phantom is fixed at the base and moved at the apex by an axel driven by a servo motor. However, the applied translation and rotation to the apex is poorly accurate, resulting in ejection fraction lower than physiologic (147) and flow patterns that are similar but not directly comparable to the *in vivo* blood flow (149). The development of myocardial structures that are soft but also active, enabled the simulation of realistic pumped blood volumes and aortic pressures (150). In (151), the myocardium of the cardiac phantom is constituted by two layers of elastomeric membranes, and it is deformed through pneumatic inflation and deflation. For the preclinical testing of intracardiac devices and the simulation of medical interventions with high degrees of realism (152), pneumatic soft artificial muscles were employed in the design of high-fidelity heart simulators. A left ventricle simulator built with latex rubber and helically oriented McKibben actuators mimicked the natural heart motion of both axial translation and apex rotation (153). A natural heart contraction was also achieved by a biorobotic hybrid heart that preserves the organic intracardiac structures of a porcine heart but substitutes the natural myocardium with a soft robotic system made with fiber-reinforced soft pneumatic muscles (154). However, the employed actuators generate lower axial contraction and higher radial expansion compared to the natural cardiac muscle fibers, thus future improvements in contractility are expected to further enhance the motion fidelity.

In the last decade, different driving principles were investigated for the development of soft peristaltic pumps whose performances are comparable to the natural heart, in first instance for simulation purposes, but also envisioning the future applicability as artificial hearts for organ assistance or even replacement. Soft peristaltic pumps were created by disposing tubular modules in series, whose individual contraction is induced by the application of a magnetic field (155) or a voltage (156). A two-module dielectric peristaltic pump which consists of short tubular pumps made by stacking dielectric membranes demonstrated a high energy density, it is quiet, light weight and can be operated at physiologically relevant frequencies (1.5 Hz). However, the low flow rate of 2.5 L/min at outflow pressures that are even four times less than physiologic, together with the required high driving voltage, highlight that there are still many challenges to be faced before considering the use of Dielectric Elastomers as active elements for the application in an artificial heart. Moreover, the combustion of gases was explored for a combustion-powered soft pump made with a room temperature vulcanizing silicone, but the system efficiency demonstrated to be low (157), and thermal and mechanical damage were registered after 30,000 combustion cycles (158). Besides efforts are still necessary to increase the pumping capabilities in physiologically relevant conditions of pressure, the pneumatic actuation is employed in dynamic simulators of the entire heart or of a single ventricle, that open the way towards their application as mechanical assistive or organ replacement devices too. In (159), a left ventricle made of an artificial myocardium created combining McKibben artificial muscles with a silicone embedding matrix is described. The actuators are arranged as the sub-epicardial layer of the natural muscular fibers and the resultant soft structure replicates both apical and basal rotations of the heart. A foam-based heart constituted of two ventricles was pneumatically driven and presented as a possible implantable prosthetic or assistive device in the near future (160). Also, a biomimetic cardiac simulator in which the artificial ventricle made of thermoplastic elastomer and polyurethane is deformed by an inflatable artificial myocardium has possible application as an artificial heart, if the materials employed for the fabrication are modified to be medical-grade (161) and still, if the device design is optimized to increase its pumping capabilities. Indeed, for the concrete evaluation of an artificial organ as a clinical option for the replacement of the natural organ, the artificial system must satisfy the physiological minimum requirements in terms of functionality, in addition to the system safety, biocompatibility and durability.

Artificial organs

The following paragraph reviews artificial organs based on soft robotics technologies, with reference to the following order of anatomic systems: sensory organs, urinary system, respiratory, and cardiovascular system. The literature research was focused on the artificial soft systems that are intended to substitute the organ for aesthetic purposes only (such as in the case of a prosthetic eye and ear), but also on soft artificial organs that aim to restore the functionality of the natural counterpart.

Sensory organs

Among the sensory organs, orbital exenteration prosthesis is used for the psychological and cosmetic rehabilitation of those patients who experienced eye and orbital contents loss. Indeed, the absence of an eye is both physically and psychologically traumatizing and can severely affect the human interactions. In (162) a complete static orbital prosthesis made of a silicone elastomer was presented. It consists of fixed eyelids, an ocular prosthesis insert, and artificial eyelashes. Three case series of three patients were analyzed with a minimum follow-up period of 6 months, demonstrating an efficient, standardized, reproducible

Figure 12 Orbital prosthesis. Republished from (163).

exenteration prosthesis. The prosthesis was produced using a fabrication workflow based on 3D scanning, computer-aided design, 3D printing, and silicone casting. This procedure requires a high level of expertise and long production time. While, in (163) an improved protocol that is both time-saving and accessible in the personalized fabrication of silicone facial prosthesis for diverse facial defect cases was developed, see Figure 12. The procedure was the combination of 3D facial scanning, digital reconstruction, and innovation of traditional silicone prosthesis production using the reproducible major mold and multiple prototypes. This resulted in an accurate and personalized facial prosthesis with accessible cost and short production period. The silicone orbital prosthesis resulted from such protocol was validated on a 71-year-old woman patient who had been diagnosed with squamous cell carcinoma of the right frontal sinus.

In the auditory system, the human ear is made of auricular cartilage with excellent mechanical strength, however, once injured, its lack of intrinsic self-repair and regenerative abilities make self-healing difficult. Recent developments in material science, bio-fabrication, 3D printing, and *in vitro* tissue engineering techniques make it possible to design and fabricate a human ear-shaped cartilage *in vitro*, for its clinical application (164). In (165), a bionic ear was generated via 3D printing of a cell-seeded hydrogel matrix in the anatomic geometry of a human ear, along with an intertwined conducting polymer consisting of infused silver nanoparticles. This method allowed the production of the biological, electronic, and structural components of the bionic organ in a single process. In other studies (166,167) CT scanning and 3D printing were employed to tackle the fabrication of a biodegradable scaffold, replicating the exact auricular 3D structure symmetrical to the patient's healthy ear and possessed good mechanical properties. In (166), after the autologous chondrocytes derived from microtia cartilage were seeded onto the scaffold and *in vitro* cultured for three months, cartilage frameworks with patient-specific ear-shape were generated and then implanted to reconstruct auricles in five patients with the longest follow-up time of 2.5 years. Whereas in (167), the auricular model was implanted subcutaneously in nude mice, showing a great prospect in the clinical application of auricle regeneration. A novel strategy to engineer auricular cartilage using Silk Fibroin (SF) and PVA hydrogel was reported in (168). In this study, different hydrogels with various ratios of SF and PVA by using salt leaching, silicone mold casting, and freeze-thawing methods were constructed. Based on the cell viability results, the authors found a blended hydrogel composed of 50% PVA and 50% SF (P50/S50) to be the most suitable hydrogel among the fabricated ones. An intact 3D ear-shaped auricular cartilage formed six weeks after the subcutaneous implantation of a chondrocyte-seeded 3D ear-shaped P50/S50 hydrogel in rats. The histological analysis showed a mature cartilage with a typical lacunar structure both *in vitro* and *in vivo*.

Urinary system

In the urinary system, the artificial bladder and the urinary sphincters have been considered. The bladder functionalities are of paramount importance to remove unnecessary fluids from the body: the ability of collecting and voiding urinary fluids in a correct manner is fundamental to help maintaining internal chemical homeostasis and prevent damage to the body. However, diseases such as cancer, neurological disorders or other pathologies can cause the partial or complete loss of bladder sensitivity and detrusor activation. In the most severe cases, radical cystectomy is the gold standard, and the entire organ is removed. The restoral of its functions is either done by urinary system diversion or organ replacement with autologous tissue from the intestine. These methods, however, significantly reduce the quality of life. In 2021, Pane et al. presented an artificial bladder system able to mimic the bladder functions (169). The device is based on a folded pocket realized with thermo-sealed polypropylene sheets, whose walls are reinforced with acetate sheets to provide stability; the maximum volume of the pocket is 260 ml. Due to the inextensible nature of the pocket, the sensing relies on magnetic distance measurements. A novel sensing strategy was proposed, that combines high-sensitivity digital tri-axial magneto-resistive sensors with planar electromagnetic coils, supplied with on-board electronics. The device was tested to assess its sensing capabilities *in vitro*, and successively implanted *ex vivo* within the pelvic cavity. Although further studies are needed to increment the sensitivity, especially during the last 60 ml filling, this is the first soft robotic artificial bladder that could fully substitute the natural counterpart.

Among the pathologies associated with the urinary system, urinary incontinence is a severe and incident pathology that

causes high discomfort and serious psychological implications to the patients. A wide range of surgical interventions are available, but in the most severe cases the implantation of an artificial sphincter is required (170). For the management of urinary incontinence, the most common technical approach consists in the implant of a controllable artificial sphincter that, placed around the urethra, squeezes and relaxes the canal to either maintain continence or allow urination (171). Common complications related to the clinical translation of these devices are mechanical failures and urethra damages, such as external surface erosion or atrophy of the area surrounded by the device (172). A preliminary study on the use of electroactive structures made from several thin layers of silicone was presented in (173). The material fast response, low dissipation factor, adequate mechanical properties and biocompatibility make it a valid candidate for the actuation of an artificial sphincter, but a validated device based on this technology is still missing. A hydraulic actuation was employed to realize an artificial urinary sphincter made of an inflatable silicone cuff, a silicone fluid reservoir and an implanted pump, to displace fluid between the first two components and, consequently, open and close the urethra lumen, in the area in which the soft cuff is positioned (172). The effectiveness of this device was demonstrated *in vitro* and *ex vivo*, on fresh pig bladders. The low complexity and the simple operation principles guarantee reliability, while the integration of a magnetic switch allows easy control. However, the magnetic switch could be operated accidentally by the presence of an external magnetic field and does not allow modulation of the pressure exerted by the cuff. In addition, no shrewdness is presented to minimize the device related risks of tissue erosion and atrophy. The *in vivo* tests conducted on an artificial urinary sphincter actuated by artificial muscles made of SMAs demonstrated that the strategy presented by the authors solves the mentioned problems of device biocompatibility and acceptability (174). Indeed, three cuffs were placed around the urethra and independently and sequentially activated to maintain continence but at the same time avoiding permanent urethra compression. A remarkable advantage of this solution is the possibility of tuning the pressure of the cuffs after implant, so that the minimum pressure needed to maintain continence is employed. The active cuffs are made by SMA (NiTiNOL), that can be repeatedly activated at low energy costs. In addition, all the components are covered by a layer of medical grade silicone to increase the biocompatibility of the surface of the device in contact with the natural tissues and fluids. The device was tested on sheep animal models for a follow-up period of three months after implant, and long-term *in vivo* studies are planned. This first phase of animal experimentation was conducted by using a percutaneous energy transfer, and a transcutaneous system is planned to be integrated in the future version of this device for clinical evaluation.

Digestive system

In addition to urinary incontinence, fecal incontinence is a very debilitating condition that strongly affects the quality of life. In the past, for the most severe cases that could not be treated with tissue repair techniques, the colostomy (an opening in the large intestine with an attached ostomy system) was the only option. The introduction of artificial anal sphincters opened novel clinical perspectives. Soft anal bands can be positioned around the anal tract, and they can be hydraulically operated to open and close the lumen of the bowel, thus restoring continence. The Artificial Anal Sphincter (AAS) is totally implanted and composed of a soft anal band, a silicone balloon as fluid reservoir, and a valve, both the latter are manually controlled. However, the clinical trials revealed that technical and surgical complications occurred in almost 50% of the involved subjects. In addition, the manual handling of the device resulted to be very difficult for some patients, that experienced pain and required the support of their relatives (175). The most studied and tested artificial sphincter is the fluid-driven Action Neosphincter (176), a device that received the FDA approval in 2001 but it was recalled in 2011 due to failures of the control pump. The exact life expectancy of this device is still unknown. There are patients with functioning devices for more than ten years after implantation, while 27% of the subjects involved in the study required early device explant for malfunctioning, infection, pain, and erosion of the soft band into the anal canal (177). The latter, together with the ischemic injury of the bowel, are recognized as device-related complications that researchers solved by minimizing the pressure that the soft band applies on the bowel (178) and by changing the squeezing mechanism from radial to sandwich, to avoid buckling of the tissue (179). The sandwich mechanism was employed in an artificial sphincter made of SMA ribbons and silicone sheets with a layered structure. At body temperature, the flat shape of the SMA ribbons close the lumen, while, upon heating, the shape change into arc enables the opening of the intestinal canal. The silicone sheets are medical-grade cushions that reduce the compressive stress to the tissues and ensure thermal insulation. The introduction of a temperature sensitive reed switch and of a mechanical hinge, to maintain the sphincter open without using any power supply, solved the previously reported issue of tissue burning (180). The artificial sphincter functionality and safety was confirmed by three months *in vivo* experiments on goats, and the clinical trials are yet to come.

Respiratory system

Looking at the respiratory system, the tracheal, the lungs and the diaphragm substitution with artificial organs are still open challenges. Human trachea can be affected by severe diseases that require a tissue reconstruction with autologous tissue or an allogenic tracheal transplant. However, at present,

they often result into difficult adaptation, lack of function or limited biocompatibility. The necessity of a definitive and biomimetic solution is thus crucial.

Although, tissue engineering techniques are fundamental to develop this specific organ, due to biocompatibility issues (181), the design principles, as variable compliance, modularity, or smart structures strongly remind of the soft robotics standards. Indeed, the main challenge that research groups faced was the reproduction of the concurrent presence of circumferential compliance and longitudinal extensibility, fundamental to develop a biomimetic tracheal segment.

To obtain these properties, modular approaches have been presented: alternating rigid and soft rings. In (182) cartilage was alternated to a porous PSeD/Polycaprolactone (PCL) biomaterial, successively stacked onto a silicone tube and implanted for vascularization. A similar approach was employed also in (183) where the best performing ratio between rigid and soft rings was investigated with the same Hydroxyethyl Methacrylate (HEMA) hydrogel but different moduli. The material was successively modified to p(MA-co-MMA) hydrogel as it was demonstrated to have lower cytotoxicity (184). Porous bellows structures were modelled (185) and tested (186) with a polymer blend of poly-(L-lactide-co-ε-caprolactone) (PLCL, molar ratio, 60:40) and gelatin (from porcine skin, G2625-500G, Sigma Aldrich, MO, USA). Carbon nanotubes PDMS-based tracheal prostheses were investigated in (187–189). A different design technique was suggested in (190) where the 3D-shape of the tracheal tube was obtained by folding a hydrogel-laden paper with origami techniques. While in (191) 3D-printed Thermoplastic Polyurethane (TPU) scaffolds were fabricated and tested *in vitro* e *in vivo* to determine performances: after 16 weeks no stenosis, tissue granulation or detachment were observed.

For what regards the lungs, in the most severe cases, the lung transplant is still the only effective treatment (192). Due to the shortage of donors, 150,000 Americans die every year from this disease, as only 2,000 lung transplants are performed annually. While waiting for a donor, extra-corporeal membrane oxygenation, nowadays, is the only viable alternative, although it presents some drawbacks, such as the need of high levels of systemic anticoagulation and the high risk of bleeding. For this reason, since the early 2000s, microfluidic-based artificial lungs have been studied. These devices typically offer the potential to drastically increase the ratio between the gas exchanging membrane surface area and blood volume, together with a more biomimetic branched design (193). Although not based on common soft robotic technologies, the usage of PDMS to create gas pathways, alternated to layers of blood microchannels, underline the potentialities of the microfabrication approaches within the field (194). The Potkay research group presented different works on the topic (195–198) and Thompson within the same group, presented in (199) the optimization of a single layer PDMS-based microfluidic artificial lung, comparing its performances to other state of the art alternatives (197,200,201) and to the NovaLung iLA Membrane ventilator.

The substitution of the natural diaphragm with an implanted artificial diaphragm to restore ventilation was investigated by a single research group and described in (202). As active element, an electroactive elastomeric sheet was used and held flat by a more rigid silicone frame. Both elements were covered by a thin film of biocompatible silicone, while a peripheral material was used for suturing the device to the residual natural muscle. In the human body, the diaphragm is flattened when it is contracted. This creates a decrease in pressure in the chest with respect to atmosphere and the lungs inflate. During exhalation, the diaphragm relaxes, and it assumes a dome shape that forces the air out of the lungs. The artificial diaphragm based on the electroactive polymers substitutes only half of the natural diaphragm and leaves intact the vessels. When a voltage is applied, the electroactive film expands and the positive abdominal pressure pushes it upwards, causing exhalation. The removal of the voltage brings the film in its rest and flattened shape, and the lungs inflate. The described device is powered transcutaneously, using an implanted induction coil. The animal trials conducted on a dog showed that the artificial diaphragm deforms as expected, but further optimizations are needed to increase the displacement capabilities of the electroactive film and thus achieve the required minimum levels of ventilation.

Cardiovascular system

In the cardiovascular system, soft artificial hearts, heart valves and vessels were studied. At the state of the art, the most advanced prosthetic soft heart device is a pneumatically driven total artificial heart. This device is intended to replace both natural ventricles with two soft chambers, actuated by an expansion chamber placed in between (203). During systole, the expansion chamber is inflated, pressing the blood from the artificial ventricles towards the natural outflow vessels. The deflation of the expansion chamber causes the shape recovery of the soft structure and the consequent passive filling of the ventricles. The softness of the employed silicone material enables a biomimetic movement of the entire structure at every heartbeat that excludes the formation of dead spots of the flow. For this reason, this device is evaluated as less thrombogenic than the traditional and rigid artificial hearts, and less amounts of anticoagulants are expected to be needed as pharmacological treatment. The most recent research focused on the device optimization in performance and durability. Besides progresses were made with respect to the previous work (203), the cardiac output of both the right and the left ventricle in physiological conditions still do not meet the clinical requirements for implant (204). Moreover, the flow rate of the two ventricles is not equal (3.95 L/min and

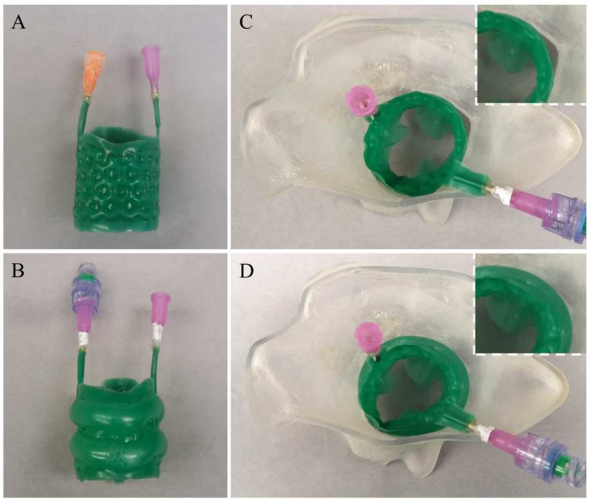

Figure 13 Transcatheter tricuspid valve repair device, based on pneumatic actuating technology. A) depressurized state B) pressurized state C) unpressurized state positioned in a 3D printed patient-specific model D) pressurized state within the model, with a better anchoring. Courtesy of Dr. Amir Ali Amiri Moghadam, Kennesaw State University, and Prof. Bobak Mosedegh, Weill Cornell Medicine, USA.

2.45 L/min for the right and the left ventricle, respectively). For the clinical applicability of the device, the right-left balancing is an aspect of major concern since an increased output of the right ventricle relative to the left ventricle causes an excess of blood volume in the lungs, called pulmonary edema. In addition, since a device longevity of several years is required, both the design and the employed materials were optimized. The finite-element method was introduced to make design modifications that minimize local stresses, while a custom made high-temperature vulcanizing silicone was developed for the fabrication of the device by injection molding in metallic molds. Indeed, the employed materials and the manufacturing technique are key aspects in determining the durability of a soft artificial heart. In (205), a device based on the same pumping mechanism but made of an extremely durable hot vulcanizing rubber by rubber compression molding demonstrated its functionality for one million cycles.

The described soft artificial hearts were tested on bench, by using experimental setups that replicate the compliance and the hydraulic resistance of the human circulation. However, before moving towards animal experimentations, these devices must be optimized and demonstrate both functionalities and durability that meet the clinical requirements.

Small caliber vascular grafts were presented in (206). The study reports good mechanical properties, sometimes also superior to the ones of natural vessels, a mass loss lower than 2% over 3 months and a great biocompatibility, when interacting with human fibroblasts.

Active soft robotic artificial valves have been investigated to guarantee the best possible match and anchoring between the implantable artificial valve and the patient body (207,208). Both the above-mentioned solutions are based on pneumatic actuating technologies. In (207), the authors analyzed the case of a tri-leaflet valve and a pneumatic anulus. The modelled valve is made of polymeric material PVA-reinforced with bacterial cellulose nanofibers which mimics the native heart valve tissues, while the anulus is designed as a ring-shaped PneuNet, casted in silicone rubber (modulus 43 kPa, shore A hardness 30 A), chosen for its comparable stretchability to the valve material. The configuration of the ring is such to increase the radius of 10% when activated. In (209), instead, an inflatable stent manufacturing is presented, and successively tested as transcatheter tricuspid valve repair device in (208), see Figure 13. The device was fabricated by thermo-sealing using a heat press sheet of TPU, with a sacrificial film of PVA. The PVA film served to obtain the pattern for the inflatable channels, and thus was successively dissolved in water. The sheets were then rolled into a cylinder and glued to secure the edges together. The tri-leaflet valve was then constructed from three pockets integrated into a cylindrical structure. PVA was used to create the pockets, and to prevent the bonding between the top TPU layer and the middle one. Finally, they were rolled into a cylinder and attached to the patterned base. The base was tested to understand its pull-out force against pressure, while the complete device into physiological flow simulator. The device was successively tested in terms of anchoring performances also in a 3D-printed tricuspid anulus, obtained through CT scan imaging (208). Although some studies are still necessary to provide stability to the device once implanted, and guarantee full biocompatibility, these studies showed relevant and promising soft robotic alternatives to artificial valve designs.

Assistive Devices

Soft robotics technologies found application also in the assistive field, for both sensing and actuation. Substituting an organ with an artificial device is, indeed, an extremely challenging task, and even if in some cases it is a viable solution, transplant is still the preferred option. Therefore, researchers presented works where the artificial device could assist the function of an organ, instead of fully substituting it.

Sensory organs

Within the sensory organs, artificial skin devices and artificial skin devices and synthetic eyes were presented as assistive systems.

Artificial skins were developed for various applications, such as wearable devices and sensorized skins for the robot

interaction with the environment. Rigid transistors containing single-walled carbon nanotubes (SWCNs) were embedded in an elastomeric matrix to create a conformable electronic skin (E-skin) that can sense and map the temperature of contacting objects (210). In another work, the carbon nanotubes were added to the polymeric network of a hydrogel to improve the temperature sensitivity of the material and create a temperature sensor (211). Artificial skins that can sense force and pressure were created by dipping tissue papers in a SWCNs solution and then embedding the obtained structure in a thin layer of PDMS (212). The device had high sensitivity, rapid response time, low power consumption (around 10 W) and it demonstrated the usability as a large-area pressure sensor (212). Several works focused on the development of artificial skin devices that can sense both strain and pressure (213) by using ionic hydrogels for their similarity to human tissues. Indeed, hydrogels are soft water-based materials which generally exhibit low interfacial tension with water, resulting in biodegradability and good biocompatibility. However, in environments with different temperatures and humidity levels, the hydrogels can suffer from drying or freezing below 0 °C (212). As for the practical application of the E-skin, the stability in time is a fundamental requirement, together with the fatigue resistance and stretchability. In addition, the self-healing capacity is a highly desirable property to increase the device similarity to human skin (213), (211). A biocompatible and stretchable polyacrylamide hydrogel containing lithium chloride salts as a ionic conductor was applied on the human skin as a 2D patch that was used to perceive various motions, such as tapping, holding, dragging and swiping (214). The extrusion-based 3D printing of hydrogels enabled the creation of a fingertip which spontaneously heals after mechanical damage and can sense the exact location of repetitive touches, with an excellent spatial resolution of 2 mm (215). Very recently, the optimization of this hydrogel composition with the addition of the organic solvent ethylene glycol provided both a long-term stability of the device (over 1,000 hours) and a very low freezing point (below -40 °C) (216). In 2021, the biocompatibility of ionic skins based on conductive hydrogels was perceived as an aspect of paramount importance towards the development of assistive devices with a high level of tissue integration (217). The last frontier of the E-skin is represented by a bio-inspired and 3D-printed hydrogel in which biomimetic gradient channels allow the transport of substances from non-living interfaces to the human body (218). The described ionic skin showed excellent biocompatibility and stability on human skins in ambient conditions. Future goals will be the creation of a crosslinked network structure to recreate the elastic fibrous network of the human skin, to further increase the mechanical similarity between the artificial and the human skin.

In (219), a human machine interface between human eyes and a soft biomimetic lens was developed, which was mainly composed of electroactive polymer films. The developed biomimetic lens contained multiple separated DE films, actuation of which were controlled by Electrooculographic (EOG) signals. EOG signals reflect the change of electrical potential difference between the cornea and the ocular fundus of eyes, which is closely associated with the eye movements. Because of the use of soft materials, the relative change of focal length of the developed lens could be as large as 32% through deformation, which was comparable to that of human eyes. The system developed in this work has the potential to demonstrate the use of EOG signals to control soft machines.

Digestive system

For the assistance of gastrointestinal tubular organs as the esophagus, assistive devices for mechanotherapy, aiming at the esophageal tract repair, were developed (220,221). The long gap esophageal atresia is a congenital defect in which the esophagus presents a gap of 3 cm or more, that prevents the bolus from reaching the stomach. In the nowadays clinical practice, the issue is solved by making an incision on the back, place sutures in the lower and upper end of the organ, and increase the length of the tissue incrementally, by tensioning

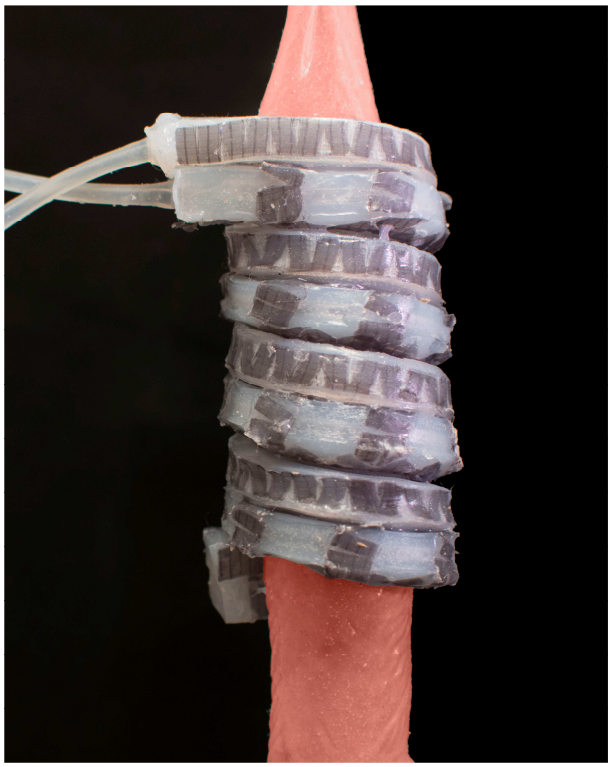

Figure 14 Soft assistive device for the esophageal tract, composed of two pneumatic strands providing different motion patterns upon pressurization. Courtesy of Dr. Eduardo R. Pérez Guagnelli, Dr. Joanna Jones and Dr. Dana Damian, University of Sheffield, UK.

it externally to the body, monitoring the process through X-ray imaging, while the patient is sedated in intensive care. First in (220) and successively in (220), the authors proposed a device able to stimulate tissue growth, that could be potentially used as implant in assisting or substituting the motion of tubular organs as stomach, intestine or esophagus. The device is a helically coiled soft actuator, composed of two pneumatic strands that due to their orientation and some wall reinforcements is able of both axial and radial expansion, see Figure 14. The main advantage of this solution is related to the modularity and multifunctionality of the device, making it easily adaptable to a large number of pathological cases. The pneumatic strands, indeed, depending on the orientation of the channel profile, are able to provide different motion outcomes. After being modelled in ABAQUS, the designed channel profile is obtained by constraining the casted silicone body Ecoflex 00-30, through laser-cut polyester sheets painted with uncured Ecoflex 00-10. The different strands, 12 cm long, are assembled with uncured Ecoflex 00-10, after being coiled around a cardboard cylinder. The axial actuation chamber expands to displace adjacent chambers, increasing the axial size of the actuator. The radial actuation chamber exhibits laterally emerging bubbles from the unconstrained sections, yielding radial expansion of the actuator. The independent and the interdependent characteristics of the actuator were evaluated in three sets of experiments, evaluating pressure and force displacement characteristics. The achieved forces are ranging up to 3 N against spatial constraints when pressurized, and maximum extension of the axial actuation chamber was evaluated as 35% of its initial length. Although further studies will be needed to better control the interdependences of the chambers to maximize their capabilities, the results seem to be promising towards the development soft robotic active implants.

Urinary system

Within the urinary system, devices aiming at assisting the bladder sensing and voiding functionalities were presented. In (222), an ultra-compliant device based on carbon nanotubes was studied and tested to sense the volume modifications and send stimuli to activate the voiding functionality. In (223) and (224) a device based on SMA actuators was designed and optimized to improve the emptying: a flexible 3D-printed vest surrounded the bladder, and SMA springs were oriented to generate compression in an efficient manner. Also, Hassani et al. (225) successively developed a solution that combined SMA-based actuation and a capacitive sensor, able to detect filling and voiding phases. The system allowed a voiding ratio ranging from 71% to 100%, without restraining the filling. A thermo-responsive system was presented by Yang et al., in this case based on a hydrogel reinforced by a silk scaffold, manufactured in a balloon-like shape (226). The device was tested *in vitro* and *in vivo*, on a rabbit.

Respiratory system

When assisting respiratory failure, the standard treatment is aiding the patients with traditional mechanical ventilators that might be connected to their mouth or through a tracheostomy. However, there are several associated comorbidities, and the quality of life is strongly affected by the limited motility. In the human body, the 70% of respiration is driven by the repetitive movement of the diaphragm, thus a pure mechanical action can be assisted or even substituted by implanted soft robotics systems. Very recently, a diaphragm assist system that works as an implantable ventilator was presented in (227). The system consists of two McKibben actuators placed on the native diaphragm and anchored at their extremities to the ribs, in an AP direction. With pressurization, the actuators shorten and push the diaphragm downward, assisting inspiration. This innovative concept was tested in a live porcine model and demonstrated the ability of augmenting relevant metrics of ventilation, such as the peak inspiratory flow and the tidal volume, that is the volume of air of one single breath. Future works are directed towards the device optimization and the integration of a portable pneumatic pump and control system, opening novel clinical options that could change the life of patients affected by respiratory failure.

Cardiovascular system

Soft robotics technologies breathed a new life also into the field of cardiac assist devices. The available Ventricular Assist Devices (VADs), indeed, still present problems related to bleeding and blood damage. For this reason, the development of non-blood contacting passive, and/or active devices able to reshape the failing hearts represented a promising alternative. Although devices as CorCap (228) were previously developed to achieve this goal, they did not become of widespread use. The introduction of novel fabrication techniques and materials represented therefore a new starting point for the field. Some devices aimed at restraining passively the heart geometry while adapting their properties at the different cardiac cycle phases (229). More frequently, instead, the assistance was also active: in (230) authors reported a magnetically actuated assistive device mounted onto a 3D-printed patch able to improve the ejection fraction of 37% in the left ventricle and 63% in the right one. Another actuating principle was instead used in (231), where the authors presented a silicone-based material embedding electrothermally-responsive fibers (Dragon Skin 10 with silver coated nylon yarn, Shieldex Trading, USA). This solution was tested in terms of pressure generation ability on a lamb heart. A device surrounding the heart and providing assistance was developed also by Mac Murray in (232). The authors presented a patient-specific design of a buckled-foam actuator: MRI and CT images were used to obtain a 3D-printed model of the studied heart. After developing a mold, polyurethane foam (Flex Foam it! III and V, Smooth-On Inc.) was casted and coated by a non-porous

layer of Vytaflex 20 (Smooth-On Inc.), the foam was buckled to amplify its compressive effect. The device was actuated through a pneumatic line. Another pneumatic direct cardiac compression device was developed by Roche et al. (233). This device was based on the use of McKibben artificial muscles (234), disposed in a bioinspired manner, to replicate the heart motion (235). The main issue encountered was the coupling and synchronization with the native heart, separately investigated in (236). The same problem was investigated also for an intracardiac device (237). Although based on pneumatic muscles (238), this device was intended to be implanted within the failing ventricle: the inflation of the actuator bring closer the ventricular walls, decreasing the internal volume. It was designed for right heart failure (239), but also tested for left heart failure (239, 240), to demonstrate its capabilities. Another example of intracardiac device, was studied by Gharale et al. (241) where a polyurethane balloon undergoes inflation/deflation cycles to improve the ventricular ejection fraction. All the presented devices highlight newly opened possibilities that soft robotics actuation technologies demonstrated within the assistive field. Although some issues frequently related to interfaces between artificial systems and failing organs need to be solved, the proposed solutions introduced a revolutionary approach to important biomedical problems that are still waiting to be untangled.

Discussion and conclusions

In the past years, growing interest started to rise around soft robotics technologies applied within the biomedical field. Indeed, the use of additive manufacturing techniques combined to new actuation strategies, enabled the development of innovative systems with unprecedented properties. High-fidelity patient-specific phantoms, bioinspired actuation patterns and artificial devices able to enhance or fully substitute the diseased counterpart are just some examples.

As visible in Figure 15, the number of studies presenting soft static simulators started to increase in 2016. Before that year, many researchers tried to replicate tissue-mimicking properties or specific organ geometries by using off-the-shelf deformable materials, as fabrics, sponges, or balloons, combined to restraining rigid elements. Lately, instead, computer-aided design and 3D printing techniques enabled the modelling and fabrication of patient-specific phantoms, with materials of tunable mechanical properties aiming at guaranteeing deformations and elastic responses similarly to the natural counterparts. The use of casted polymeric materials, such as elastomers and hydrogels, became therefore of widespread use for the design of platforms for surgical rehearsal, despite some common challenges in fabrication as the correct alignment of parts, or the difficulties of retrieving high-fidelity models of moving organs.

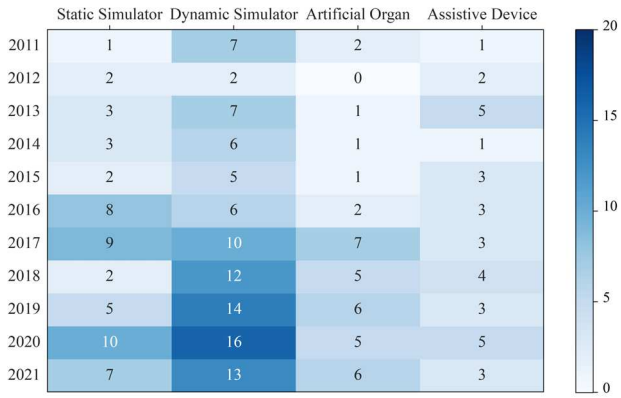

Figure 15 Distribution of the analyzed articles that were published between 2011 and 2021, divided per category (static/dynamic simulator, artificial organ, and assistive device).

The combination of deformable materials with specific soft actuator typologies also enabled the development of soft dynamic simulators. Besides decreasing the overall number of animal studies, these systems aimed also at fully understanding the dynamics of specific active organs, e.g. the esophagus or the stomach, or the implications of motion on passive ones, as the lungs or the heart valves. The highest number of analyzed articles (98 out of 219 belong to this category.

The success reported by these dynamic systems, paved the way towards the development of a new generation of implants: complex soft actuated devices, as assistive mechanisms, and artificial organs, that for the first time were designed to be in close contact with body tissues.

The introduction of deformable structures and biomimetic motions, enabled to obtain encouraging results despite the early stages of research. However, these systems generally lack of biocompatible interfaces, usually leading to relevant and hardly controllable immune responses. Moreover, much more information could be acquired, and a better control strategy could be implemented by embedding reliable soft sensors. To date, however, very few technologies are available to monitor specific parameters without impeding or restraining the overall range of motion, therefore also decreasing the average life of such devices.

These considerations are reflected also into the maximum technological readiness level (TRL) of the presented studies, which generally stands underneath 4. By taking inspiration from the TRL levels, it was possible for each organ to categorize the systems in terms of Level of Development (LoD) as in Figure 16. This additional parameter allows a more specific description level, tailored on the application field. Level 1 corresponds to articles where basic principles are observed, in terms of soft component development (material, actuator or sensor); Level 2, instead, introduces a soft system demonstrated as proof-of-concept with tests conducted in a laboratory environment; Level 3 groups

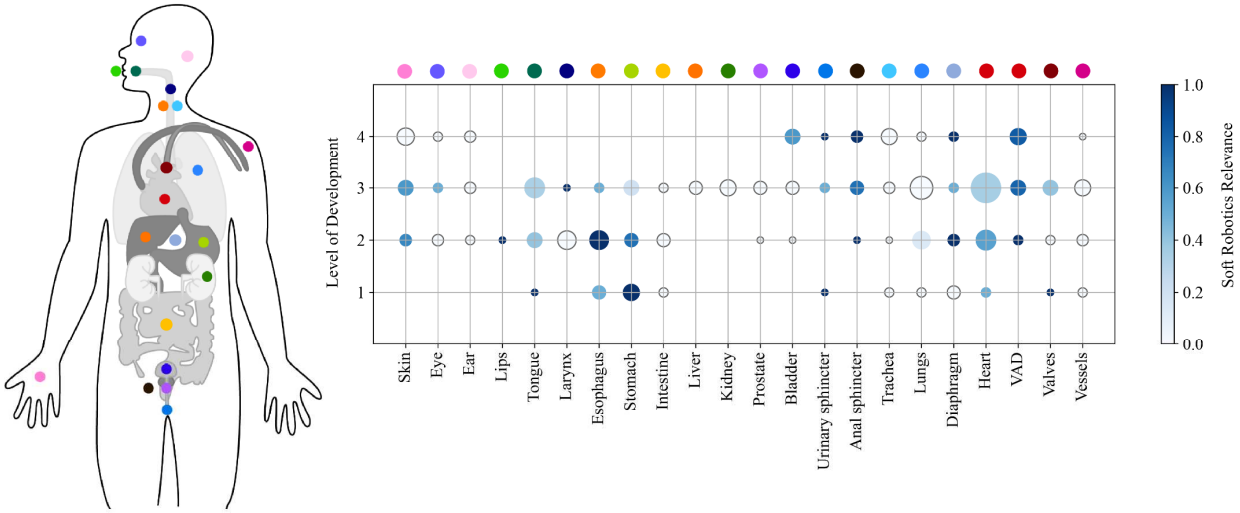

Figure 16 Level of development (from 1 to 4) of each artificial organ. The dimension of circle is proportional to the number of articles, while the color scale indicates the soft robotic relevance.

devices tested in relevant environments with *in vitro* tests, while Level 4 articles report demonstrations through *in vivo* studies. The dimension of each marker in Figure 16 is proportional to the number of articles referring to the specific organ and its position is related to its LoD. Most of the analyzed articles are clustered between LoD 2 and 3, underlining that soft robotics technologies are still in an initial developmental phase, but they are starting to approach different *in vitro* evaluations.

In the same figure, the color of the marker is linked to another parameter: the Soft Robotic Relevance (SRR) of the reported study. Each analyzed article was, indeed, assigned with a score from 1 to 3, corresponding respectively to 1 only for the use of soft deformable materials, 2 for the engineering of particular material properties and 3 for the presence of a deformable matter, actuated through a soft actuating technology. The displayed color therefore was obtained by mapping the ratio between the articles with SRR 3 with respect to the total of the specific marker, within a color scale (as in Figure 16).

This parameter allows to distinguish not only the dynamic organs from the static ones, as the latter will obviously have a lighter color (lower number of articles with SRR equal to 3), but also the organs for which the soft robotics actuation technologies enabled a higher LoD device, as it is in the case of the sphincters or the assistive devices for the heart.

In parallel, the diagram unravels the current developmental trends, i.e. cardiovascular devices, and the ones that so far were not yet widely investigated, but with high potential to be developed with soft robotic technologies, i.e. the diaphragm. In addition, the diagram shows that, among the organs with maximum LoD 3, the ones that have motility as primary function, such as the tongue and the heart, have greater potential of reaching the higher level of development, also considering the strong contribution of the soft robotics technologies (as highlighted by the SRR index). On the other hand, the soft robotics contribution to the development of the organs whose primary function involves biochemical processes such as during digestion (i.e. stomach, liver and kidney) is limited.

Focusing on dynamic systems, their distribution among the different levels of development in terms of presented actuating solutions is depicted in Figure 17A. This diagram confirms that most of the analyzed articles are categorized within LoD 2 and 3. In parallel, however, another important information can be retrieved: the most common soft actuation strategy is the fluidic one, with a particular preference for pneumatic systems. This activation methodology is widely employed in all the considered device categories (synthetic simulators, artificial organs, and implantable assistive devices). On the contrary, the second most preferred actuation technique, the electromechanical one, is usually employed just in case of dynamic simulators. In fact, this more traditional motion strategy employs cables and/or motors, that allow the discrete activation of specific parts of the systems or their overall reorientation in space, however resulting unsuitable in terms of implantability.

The least common actuation strategy is instead combustion, present just in LoD 2. While this approach is very effective in terms of response time and induced deformation, it is difficult to control, and it is associated to high temperature and loud operational conditions. Technologies based on electrical activation as electromagnetic, electrothermal and dielectric strategies are, instead, unusual, but more constant in number among the different levels of development. They bring the general advantage of direct activation through electric current

or voltage, but they have some drawbacks (e.g., heaviness and relatively high current of electromagnet, low efficiency and difficult temperature management of electrothermal, high voltages of dielectric actuators) that prevent them to be more widely adopted.

It is worth to mention that the use of SMAs, another electrically activated strategy, was found in the highest LoD 3 and 4, especially for the development of bladder assistive devices.

One of the reasons behind the extensive use of fluidic strategies in all the levels of the development, besides their intrinsic safety, is the wide range of available technological implementations, as visible in Figure 17B. By taking in consideration all the fluidic technologies, both pneumatic and hydraulic, at least 5 types of systems were identified. Frequently, the conceived devices are based on the actuation of a deformable membrane able to displace upon pressurization: they represent 35.5% of the total number of fluidic solutions. In parallel, however, also PneuNets and fiber-reinforced actuators as inverse pneumatic muscles or McKibben actuators are common, due to their renowned muscle-like characteristics (23.7% in both cases). Pouches, actuated foams, or other solutions are instead representing a minority (6.6%, 5.3% and 5.3% respectively). It is therefore evident that fluidic solutions were confirmed to be the most investigated soft actuation technology. The main reason behind this trend lies not only in their ease in fabrication and implementation, but also in the possibility of fully exploiting the deformability of materials. Indeed, they allow the development of smart structures, characterized by embedded actuation and tunable mechanical properties, as it is in the natural systems. Other soft actuation solutions, instead, frequently introduce rigid interfaces that limit the overall performances of the devices. One of the main limitations of soft fluidically-actuated robots is still, however, the need of bulky external supply systems that on the one hand might enable the development of simulators, but on the other might restrain the implantability of artificial organs and assistive devices. The main intrinsic limitation of fluidically driven systems is represented by the fluidic source. Soft fluidic actuators are generally studied without considering that the transductor (from electric to mechanical domain) is located remotely. There are several alternatives, such as compressed fluid reservoir, monoporpellent decomposition, and miniaturized sytems, but the main solution adopted so far is still an off-board compressor. This represents a fundamental issue for implantability, leading to solutions where the implanted system is transcutanously connected to an external fluidic source. However, this implies limitations in portability. This challenge in future could be overcome by joining forces with the microfluidic field knowledge, enabling the design of smart deformable structures powered by lower pressures and high-efficiency flow profiles.

Another field that might fruitfully contribute towards the development of successful soft implants, is the tissue-engineering one, potentially enabling the generation of biohybrid devices able to couple bioinspired motions and biocompatible interfaces.

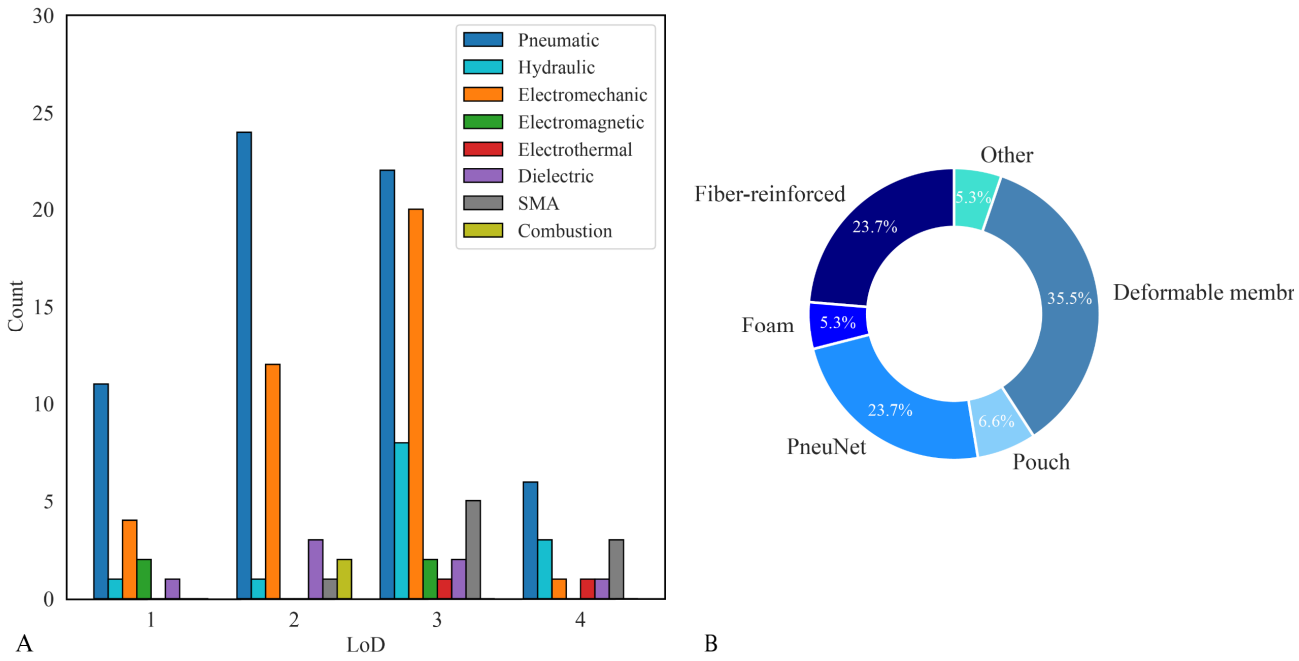

Figure 17 A) Actuation strategy distribution among different levels of development B) Distribution of fluidic actuation strategies (hydraulic and pneumatic) in the sub-categories (deformable membrane, pouch, PneuNet, foam, fiber-reinforced).

Studies in material science ranging from biomaterials to soft polymers are therefore fundamental for the future of soft robotic biomedical applications. Indeed, although the most commonly employed elastomers for 3D printing applications enabled the fabrication of high-fidelity phantoms, some specific mechanical properties of natural tissues still cannot be replicated, leading at lack of realistic feeling during testing. Moreover, self-healing materials still present biocompatibility issues, that prevent their use in the development of assistive devices or organs able to repair themselves upon rupture.

Despite these challenges, the soft robotics field is still providing, year after year, innovative solutions to important biomedical problems, giving new perspectives to the field. In future, a deeper connection with other cutting-edge research areas as material science and tissue engineering could enable the development of extremely realistic phantoms and biohybrid artificial organs, potential game-changing solutions in the medical robotics field.

Supplementary Material

Table SSS - Static Synthetic Simulators
Table DPS - Dynamic Passive Simulators
Table DAS - Dynamic Active Simulators
Table AO - Artificial Organs
Table AD – Assistive Devices

References

1. Laschi C, Mazzolai B, Cianchetti M. Soft robotics: Technologies and systems pushing the boundaries of robot abilities. Sci Robot. 2016;1(1):1–12.
2. Mussi E, Servi M, Facchini F, Carfagni M, Volpe Y. A computer-aided strategy for preoperative simulation of autologous ear reconstruction procedure. Int J Interact Des Manuf. 2021 Mar 1;15(1):77–80.
3. Berens AM, Newman S, Bhrany AD, Murakami C, Sie KCY, Zopf DA. Computer-Aided Design and 3D Printing to Produce a Costal Cartilage Model for Simulation of Auricular Reconstruction. In: Otolaryngology - Head and Neck Surgery (United States). SAGE Publications Inc.; 2016. p. 356–9.
4. Sandeep Reddy C, Rajesh M Hegde. Design and Development of Bionic Ears for Rendering Binaural Audio. In: 2016 International Conference on Signal Processing and Communications (SPCOM) IEEE. 2016. p. 1–5.
5. Ferlay J, Soerjomataram I, Dikshit R, Eser S, Mathers C, Rebelo M, et al. Cancer incidence and mortality worldwide: Sources, methods and major patterns in GLOBOCAN 2012. Int J Cancer. 2015;136(5):E359–86.
6. Finocchiaro M, Valdivia PC, Hernansanz A, Marino N, Amram D, Casals A, et al. Training simulators for gastrointestinal endoscopy: Current and future perspectives. Cancers (Basel). 2021;13(6):1–26.
7. Noda K, Kitada T, Suzuki Y, Colvin HS, Hata T, Mizushima T. A novel physical colonoscopy simulator based on analysis of data from computed tomography colonography. Surg Today. 2017;47(9):1153–62.
8. Manual I. Colonoscope Training Model 大腸内視鏡トレーニングモデル. Simulation.
9. Start BY, Membrane SA, Technique I, Tips T, Training A, Parts R. NKS Colonoscope Training Simulator Manufacturer ' s Note.
10. Walczak DA, Grajek M, Walczak PA, Massopust R, Pasieka Z, Maciejewski A, et al. The first homemade colonoscopy trainer. 2017;
11. Berger-Richardson D, Kurashima Y, Von Renteln D, Kaneva P, Feldman LS, Fried GM, et al. Description and Preliminary Evaluation of a Low-Cost Simulator for Training and Evaluation of Flexible Endoscopic Skills. Surg Innov. 2016;23(2):183–8.
12. Jones MW, Deere MJ, Harris JR, Chen AJ, Henning WH. Fabrication of an inexpensive but effective colonoscopic simulator. J Soc Laparoendosc Surg. 2017;21(2):1–4.
13. Tan X, Li D, Jeong M, Yu T, Ma Z, Afat S, et al. Soft Liver Phantom with a Hollow Biliary System. Ann Biomed Eng. 2021;49(9):2139–49.
14. Opik R, Hunt A, Ristolainen A, Aubin PM, Kruusmaa M. Development of High Fidelity Liver and Kidney Phantom Organs for Use with Robotic Surgical Systems. 2012 4th IEEE RAS EMBS Int Conf Biomed Robot Biomechatronics. 2012;(June):425–30.
15. Pacioni A, Carbone M, Freschi C, Viglialoro R, Ferrari V, Ferrari M. Patient-specific ultrasound liver phantom: materials and fabrication method. Int J Comput Assist Radiol Surg [Internet]. 2015;10(7):1065–75. Available from: http://dx.doi.org/10.1007/s11548-014-1120-y
16. Chmarra MK, Hansen R, Mårvik R, Langø T. Multimodal Phantom of Liver Tissue. PLoS One. 2013;8(5):1–9.
17. Colvill E, Krieger M, Bosshard P, Steinacher P, Rohrer BA, Schnidrig, et al. Anthropomorphic phantom for deformable lung and liver CT and MR imaging for radiotherapy. Phys Med Biol. 2020;(111):0–13.
18. Hunt A, Ristolainen A, Ross P, Öpik R, Krumme A, Kruusmaa M. Low cost anatomically realistic renal biopsy phantoms for interventional radiology trainees. Eur J Radiol [Internet]. 2012;82(4):594–600. Available from: http://dx.doi.org/10.1016/j.ejrad.2012.12.020
19. Vargasa J, Lea P, Shahedia M, Gahanb J, Johnsonb B, Dormera JD, et al. A complex dual-modality kidney phantom for renal biopsy studies. Lancet Gastroenterol Hepatol. 2020;5(6):537–547.
20. Adams F, Qiu T, Mark A, Fritz B, Kramer L, Schlager D, et al. Soft 3D-Printed Phantom of the Human Kidney with Collecting System. Ann Biomed Eng. 2017;45(4):963–72.
21. Song T, Jiang B, Li Y, Ji Z, Zhou H, Jiang D, et al. Self-healing Materials : A Review of Recent Developments. ES Mater Manuf. 2021;1–19.
22. Li D, Suarez-Ibarrola R, Choi E, Jeong M, Gratzke C, Miernik A, et al. Soft Phantom for the Training of Renal Calculi Diagnostics and Lithotripsy. Proc Annu Int Conf IEEE Eng Med Biol Soc EMBS. 2019;3716–9.
23. Boutet J, Herve L, Debourdeau M, Guyon L, Peltie P, Dinten J-M, et al. Bimodal ultrasound and fluorescence approach for prostate cancer diagnosis. J Biomed Opt. 2009;14(6).
24. Hungr N, Long JA, Beix V, Troccaz J. A realistic deformable prostate phantom for multimodal imaging and needle-insertion procedures. Med Phys. 2012;39(4):2031–41.
25. Bauer DF, Adlung A, Brumer I, Golla AK, Russ T, Oelschlegel E, et al. An anthropomorphic pelvis phantom for MR-guided prostate interventions. Magn Reson Med.

2022;87(3):1605–12.
26. Choi E, Adams F, Palagi S, Gengenbacher A, Schlager D, Müller PF, et al. A High-Fidelity Phantom for the Simulation and Quantitative Evaluation of Transurethral Resection of the Prostate. Ann Biomed Eng. 2020;48(1):437–46.
27. Gautam UC, Pydi YS, Selladurai S, Das CJ, Thittai AK, Roy S, et al. A Poly-vinyl Alcohol (PVA)-based phantom and training tool for use in simulated Transrectal Ultrasound (TRUS) guided prostate needle biopsy procedures. Med Eng Phys [Internet]. 2021;96(August):46–52. Available from: https://doi.org/10.1016/j.medengphy.2021.08.008
28. Choi E, Waldbillig F, Jeong M, Li D, Goyal R, Weber P, et al. Soft Urinary Bladder Phantom for Endoscopic Training. Ann Biomed Eng. 2021;49(9):2412–20.
29. Hackner R, Suarez-Ibarrola R, Qiu T, Lemke N, Pohlmann P-F, Wilhelm K, et al. Panoramic Imaging Assessment of Different Bladder Phantoms - An Evaluation Study. Clin Challenges Urol. 2021;
30. Lurie KL, Smith GT, Khan SA, Liao JC, Bowden AK. Three-dimensional, distendable bladder phantom for optical coherence tomography and white light cystoscopy. J Biomed Opt. 2014;19(03):1.
31. Stather DR, Lamb CR, Tremblay A. Simulation in Flexible Bronchoscopy and Endobronchial Ultrasound. 2011;18(3):247–56.
32. Hsiung GE, Schwab B, O'Brien EK, Gause CD, Hebal F, Barsness KA, et al. Preliminary Evaluation of a Novel Rigid Bronchoscopy Simulator. J Laparoendosc Adv Surg Tech. 2017;27(7):737–43.
33. Reighard CL, Green K, Powell AR, Rooney DM, Zopf DA. Development of a high fidelity subglottic stenosis simulator for laryngotracheal reconstruction rehearsal using 3D printing. Int J Pediatr Otorhinolaryngol. 2019;124(June):134–8.
34. Parsa H, Karac A, Ivankovic A. A novel surrogate lung material for impact studies: Development and testing procedures. J Biomech. 2017;63:74–81.
35. Danelson KA, Gayzik FS, Stern AR, Hoth JJ, Stitzel JD. Design, development, and analysis of a surrogate for pulmonary injury prediction. Ann Biomed Eng. 2011;39(10):2560–7.
36. Perrin RL, Zakova M, Peroni M, Bernatowicz K, Bikis C, Knopf AK, et al. An anthropomorphic breathing phantom of the thorax for testing new motion mitigation techniques for pencil beam scanning proton therapy. Phys Med Biol. 2017;62(6):2486–504.
37. Hazelaar C, Van Eijnatten M, Dahele M, Wolff J, Forouzanfar T, Slotman B, et al. Using 3D printing techniques to create an anthropomorphic thorax phantom for medical imaging purposes. Med Phys. 2018;45(1):92–100.
38. Zimmermann JM, Steffen OJ, Vicentini L, Schmid Daners M, Taramasso M, Maisano F, et al. Novel augmented physical simulator for the training of transcatheter cardiovascular interventions. Catheter Cardiovasc Interv. 2020;95(6):1202–9.
39. Tsai SL, Seslar SP. Initial experience with a novel pericardiocentesis training simulator incorporating a three-dimensional printed cardiac model. J Innov Card Rhythm Manag. 2021;12(6):4551–5.
40. Osada H, Ho WJ, Yamashita H, Yamazaki K, Ikeda T, Minatoya K, et al. Novel device prototyping for endoscopic cell sheet transplantation using a three-dimensional printed simulator. Regen Ther [Internet]. 2020;15:258–64. Available from: https://doi.org/10.1016/j.reth.2020.10.007
41. Alves N, Kim A, Tan J, Hwang G, Javed T, Neagu B, et al. Cardiac Tissue-Mimicking Ballistic Gel Phantom for Ultrasound Imaging in Clinical and Research Applications. Ultrasound Med Biol. 2020;46(8):2057–69.
42. Khairi NA, Adib MAHM, Sukri NNM, Sahat IM, Hasni NHM. The CardioVASS Heart Model: Comparison of Biomaterials between TPU Flex and Soft Epoxy Resin for Biomedical Engineering Application. IEEE EMBS Conf Biomed Eng Sci. 2020;224–9.
43. Korn L, Lyra S, Rüschen D, Telyshev D, Leonhardt S, Walter M. in silico and in vitro conductivity models of the left heart ventricle. J Electr Bioimpedance. 2020;11(May):62–71.
44. Scanlan AB, Nguyen A V, Ilina A, Lasso A, Cripe L, Jegatheeswaran A, et al. Comparison of 3D Echocardiogram-Derived 3D Printed Valve Models to Molded Models for Simulated Repair of Pediatric Atrioventricular Valves. Pediatr Cardiol [Internet]. 2018;39(3):538–47. Available from: http://dx.doi.org/10.1007/s00246-017-1785-4
45. Vukicevic M, Puperi DS, Jane Grande-Allen K, Little SH. 3D Printed Modeling of the Mitral Valve for Catheter-Based Structural Interventions. Ann Biomed Eng. 2017;45(2):508–19.
46. Stepniak K, Ursani A, Paul N, Naguib H. Development of a phantom network for optimization of coronary artery disease imaging using computed tomography. Biomed Phys Eng Express. 2019;5(4).
47. Knoops PGM, Biglino G, Hughes AD, Parker KH, Xu L, Schievano S, et al. A Mock Circulatory System Incorporating a Compliant 3D-Printed Anatomical Model to Investigate Pulmonary Hemodynamics. Artif Organs. 2017;41(7):637–46.
48. Maragiannis D, Jackson MS, Igo SR, Schutt RC, Connell P, Grande-Allen J, et al. Replicating Patient-Specific Severe Aortic Valve Stenosis with Functional 3D Modeling. Circ Cardiovasc Imaging. 2015;8(10):1–8.
49. Cloonan AJ, Shahmirzadi D, Li RX, Doyle BJ, Konofagou EE, McGloughlin TM. 3D-printed tissue-mimicking phantoms for medical imaging and computational validation applications. 3D Print Addit Manuf. 2014;1(1):14–23.
50. Kwon J, Ock J, Kim N. Mimicking the Mechanical Properties of Aortic Tissue Realistic Phantom. 2020;
51. Haghiashtiani G, Qiu K, Sanchez JDZ, Fuenning ZJ, Nair P, Ahlberg SE, et al. 3D printed patient-specific aortic root models with internal sensors for minimally invasive applications. Sci Adv. 2020;6(35):1–13.
52. Qian Z, Wang K, Liu S, Zhou X, Rajagopal V, Meduri C, et al. Quantitative Prediction of Paravalvular Leak in Transcatheter Aortic Valve Replacement Based on Tissue-Mimicking 3D Printing. JACC Cardiovasc Imaging. 2017;10(7):719–31.
53. Wang K, Wu C, Qian Z, Zhang C, Wang B, Vannan MA. Dual-material 3D printed metamaterials with tunable mechanical properties for patient-specific tissue-mimicking phantoms. Addit Manuf [Internet]. 2016;12:31–7. Available from: http://dx.doi.org/10.1016/j.addma.2016.06.006
54. Ripley B, Kelil T, Cheezum MK, Goncalves A, Di Carli

MF, Rybicki FJ, et al. 3D printing based on cardiac CT assists anatomic visualization prior to transcatheter aortic valve replacement. J Cardiovasc Comput Tomogr [Internet]. 2016;10(1):28–36. Available from: http://dx.doi.org/10.1016/j.jcct.2015.12.004
55. Biglino G, Verschueren P, Zegels R, Taylor AM, Schievano S. Rapid prototyping compliant arterial phantoms for in-vitro studies and device testing. J Cardiovasc Magn Reson. 2013;15(1):1–7.
56. Morup SD, Stowe J, Precht H, Gervig MH, Foley S. Design of a 3D printed coronary artery model for CT optimization. Radiography. 2021;(28):426–32.
57. Zeng H, Wani OM, Wasylczyk P, Kaczmarek R, Priimagi A. Self-Regulating Iris Based on Light-Actuated Liquid Crystal Elastomer. Adv Mater. 2017 Aug 11;29(30).
58. Manti M, Cianchetti M, Nacci A, Ursino F, Laschi C. A biorobotic model of the human larynx. In: Proceedings of the Annual International Conference of the IEEE Engineering in Medicine and Biology Society, EMBS. Institute of Electrical and Electronics Engineers Inc.; 2015. p. 3623–6.
59. Conte A, Maselli M, Nacci A, Manti M, Galli J, Paludetti G, et al. Conductive Silicone Vocal Folds Reproducing Electroglottographic Signal in Pathophysiological Conditions. IEEE Trans Med Robot Bionics. 2021 May 1;3(2):337–48.
60. Kniesburges S, Birk V, Lodermeyer A, Schützenberger A, Bohr C, Becker S. Effect of the ventricular folds in a synthetic larynx model. J Biomech. 2017 Apr 11;55:128–33.
61. Syndergaard KL, Dushku S, Thomson SL. Electrically conductive synthetic vocal fold replicas for voice production research. J Acoust Soc Am. 2017 Jul;142(1):EL63–8.
62. Pickup BA, Thomson SL. Flow-induced vibratory response of idealized versus magnetic resonance imaging-based synthetic vocal fold models. J Acoust Soc Am. 2010;128(3):EL124.
63. Drechsel JS, Thomson SL. Influence of supraglottal structures on the glottal jet exiting a two-layer synthetic, self-oscillating vocal fold model. J Acoust Soc Am. 2008 Jun;123(6):4434–45.
64. Murray PR, Thomson SL. Synthetic, multi-layer, self-oscillating vocal fold model fabrication. J Vis Exp. 2011;(58).
65. Romero RGT, Colton MB, Thomson SL. 3D-Printed Synthetic Vocal Fold Models. J Voice. 2021 Sep 1;35(5):685–94.
66. Shin DS, Kang SH, Kim KH, Kim TH, Kim DS, Chung JB, et al. Development of a deformable lung phantom with 3D-printed flexible airways. Med Phys. 2020;47(3):898–908.
67. Shin D-S, Kang S-H, Kim D-S, Kim T-H, Kim K-H, Koo H-J, et al. Development of an Advanced Deformable Phantom to Analyze Dose Differences due to Respiratory Motion. Prog Med Phys. 2017;28(1):1.
68. Mayer R, Liacouras P, Thomas A, Kang M, Lin L, Simone CB. 3D printer generated thorax phantom with mobile tumor for radiation dosimetry. Rev Sci Instrum. 2015;86(7).
69. Chang J, Suh T, Lee D, Cho G. SU-FF-I-104: Development of a Deformable Lung Phantom for the Evaluation of Deformable Registration. In: Medical Physics. 2009. p. 2458.
70. Serban M, Heath E, Stroian G, Collins DL, Seuntjens J. A deformable phantom for 4D radiotherapy verification: Design and image registration evaluation. Med Phys. 2008;35(3):1094–102.
71. Kashani R, Lam K, Litzenberg D, Balter J. Technical note: A deformable phantom for dynamic modeling in radiation therapy. Med Phys. 2007;34(1):199–201.
72. Nioutsikou E, Richard N Symonds-Tayler J, Bedford JL, Webb S. Quantifying the effect of respiratory motion on lung tumour dosimetry with the aid of a breathing phantom with deforming lungs. Phys Med Biol. 2006;51(14):3359–74.
73. Black DG, Yazdi YO, Wong J, Fedrigo R, Uribe C, Kadrmas DJ, et al. Design of an anthropomorphic PET phantom with elastic lungs and respiration modeling. Med Phys. 2021;48(8):4205–17.
74. Fujii M, Onoyama T, Ikebuchi Y, Uehara K, Koga A, Ueki M, et al. A novel humanoid-robot simulator for colonoscopy. Endoscopy. 2021;53(8):E291–2.
75. Formosa GA, Prendergast JM, Peng J, Kirkpatrick D, Rentschler ME. A Modular Endoscopy Simulation Apparatus (MESA) for Robotic Medical Device Sensing and Control Validation. IEEE Robot Autom Lett. 2018;3(4):4054–61.
76. Ginty OK, Moore JM, Xu Y, Xia W, Fujii S, Bainbridge D, et al. Dynamic Patient-Specific Three-Dimensional Simulation of Mitral Repair: Can We Practice Mitral Repair Preoperatively? Innov Technol Tech Cardiothorac Vasc Surg. 2018;13(1):11–22.
77. Ginty OK, Moore JT, Eskandari M, Carnahan P, Lasso A, Jolley MA, et al. Dynamic, patient-specific mitral valve modelling for planning transcatheter repairs. Int J Comput Assist Radiol Surg. 2019;14(7):1227–35.
78. Boone N, Nam HH, Moore JT, Carnahan P, Ginty O, Herz C, et al. Patient-specific, dynamic models of hypoplastic left heart syndrome tricuspid valves for simulation and planning. In 2020. p. 79.
79. Minato T, Yoshikawa Y, Noda T, Ikemoto S, Ishiguro H, Asada M. CB2: A child robot with biomimetic body for cognitive developmental robotics. Proc 2007 7th IEEE-RAS Int Conf Humanoid Robot HUMANOIDS 2007. 2007;557–62.
80. Tadesse Y, Priya S, Stephanou H, Popa D, Hanson D. Piezoelectric actuation and sensing for facial robotics. Ferroelectrics. 2006;345(December):13–25.
81. Hara F, Akazawa H, Kobayashi H. Realistic facial expressions by SMA driven face robot. Proc - IEEE Int Work Robot Hum Interact Commun. 2001;504–11.
82. Tadesse Y, Hong D, Priya S. Twelve degree of freedom baby humanoid head using shape memory alloy actuators. J Mech Robot. 2011;3(1):1–18.
83. Kobayashi H, Ichikawa Y, Senda M, Shiiba T. Toward rich facial expression by face robot. MHS 2002 - Proc 2002 Int Symp Micromechatronics Hum Sci. 2002;139–45.
84. Usui Y, Niiyama R, Kuniyoshi Y. Anthropomorphic Face Robot having Soft Mouth Mechanism with Embedded Artificial Facial Muscles. MHS 2019 - 30th 2019 Int Symp Micro-NanoMechatronics Hum Sci. 2019;
85. Hashimoto T, Hitramatsu S, Tsuji T, Kobayashi H. Development of the face robot SAYA for rich facial expressions. 2006 SICE-ICASE Int Jt Conf. 2006;5423–8.
86. Carpi F, Frediani G, Turco S, De RD. Bioinspired tunable lens with muscle-like electroactive elastomers. Adv Funct Mater. 2011 Nov 8;21(21):4152–8.

87. Pieroni M, Lagomarsini C, De Rossi D, Carpi F. Electrically tunable soft solid lens inspired by reptile and bird accommodation. Bioinspiration and Biomimetics. 2016 Oct 26;11(6).
88. Wang Y, Li P, Gupta U, Ouyang J, Zhu J. Tunable Soft Lens of Large Focal Length Change. Soft Robot. 2021 Aug 12;
89. Ng GCF, Gray-Stuart EM, Morgenstern MP, Jones JR, Grigg NP, Bronlund JE. The slip extrusion test: A novel method to characterise bolus properties. J Texture Stud. 2017;48(4):294–301.
90. Redfearn A, Hanson B. A Mechanical Simulator of Tongue-Palate Compression to Investigate the Oral Flow of Non-Newtonian Fluids. IEEE/ASME Trans Mechatronics. 2018;23(2):958–65.
91. Hayoun P, Engmann J, Mowlavi S, Le Reverend B, Burbidge A, Ramaioli M. A model experiment to understand the oral phase of swallowing of Newtonian liquids. J Biomech [Internet]. 2015;48(14):3922–8. Available from: http://dx.doi.org/10.1016/j.jbiomech.2015.09.022
92. Mackley MR, Tock C, Anthony R, Butler SA, Chapman G, Vadillo DC. The rheology and processing behavior of starch and gum-based dysphagia thickeners. J Rheol (N Y N Y). 2013;57(6):1533–53.
93. Mowlavi S, Engmann J, Burbidge A, Lloyd R, Hayoun P, Le Reverend B, et al. In vivo observations and in vitro experiments on the oral phase of swallowing of Newtonian and shear-thinning liquids. J Biomech [Internet]. 2016;49(16):3788–95. Available from: http://dx.doi.org/10.1016/j.jbiomech.2016.10.011
94. Marconati M, Raut S, Burbidge A, Engmann J, Ramaioli M. An in vitro experiment to simulate how easy tablets are to swallow. Int J Pharm [Internet]. 2018;535(1–2):27–37. Available from: https://doi.org/10.1016/j.ijpharm.2017.10.028
95. Noh Y, Wang C, Tokumoto M, Matsuoka Y, Chihara T, Ishii H, et al. Development of the airway Management Training System WKA-5: Improvement of mechanical designs for high-fidelity patient simulation. 2012 IEEE Int Conf Robot Biomimetics, ROBIO 2012 - Conf Dig. 2012;1224–9.
96. Noh Y, Segawa M, Sato K, Wang C, Ishii H, Solis J, et al. Development of a robot which can simulate swallowing of food boluses with various properties for the study of rehabilitation of swallowing disorders. Proc - IEEE Int Conf Robot Autom. 2011;4676–81.
97. Fujiso Y, Perrin N, van der Giessen J, Vrana NE, Neveu F, Woisard V. SwAlL-E: A robotic in-vitro simulation of human swallowing. PLoS One. 2018;13(12):1–15.
98. Endo N. Deformation model and experimental evaluation of a contractable and bendable wire-pulling mechanism with embedded soft tubes for a robotic tongue. ROBOMECH J [Internet]. 2021;8(1). Available from: https://doi.org/10.1186/s40648-021-00193-6
99. Lu X, Xu W, Li X. A Soft Robotic Tongue-Mechatronic Design and Surface Reconstruction. IEEE/ASME Trans Mechatronics. 2017;22(5):2102–10.
100. Marconati M, Pani S, Engmann J, Burbidge A, Ramaioli M. A soft robotic tongue to develop solutions to manage swallowing disorders. Med Phys [Internet]. 2020;1–19. Available from: http://arxiv.org/abs/2003.01194
101. Rodriguez S, Galvan R, Ganta D. Modelling and simulation of soft robotic human tongue with improved motion. Eng Res Express. 2021;3(4).
102. Gong N, Jin H, Sun S, Mao S, Li W, Zhang S. A bionic soft tongue driven by shape memory alloy and pneumatics. Bioinspiration and Biomimetics. 2021;16(5).
103. Chen FJ, Dirven S, Xu WL, Li XN. Soft actuator mimicking human esophageal peristalsis for a swallowing robot. IEEE/ASME Trans Mechatronics. 2014;19(4):1300–8.
104. Dirven S, Xu W, Cheng LK. Sinusoidal peristaltic waves in soft actuator for mimicry of esophageal swallowing. IEEE/ASME Trans Mechatronics. 2015;20(3):1331–7.
105. Bhattacharya D, Ali SJV, Cheng LK, Xu W. RoSE: A Robotic Soft Esophagus for Endoprosthetic Stent Testing. Soft Robot. 2021;8(4):397–415.
106. Dirven S, Chen F, Xu W, Bronlund JE, Allen J, Cheng LK. Design and characterization of a peristaltic actuator inspired by esophageal swallowing. IEEE/ASME Trans Mechatronics. 2014;19(4):1234–42.
107. Dang Y, Stommel M, Cheng LK, Xu W. A Soft Ring-Shaped Actuator for Radial Contracting Deformation: Design and Modeling. Soft Robot. 2019;6(4):444–54.
108. Li H, Yao J, Liu C, Zhou P, Xu Y, Zhao Y. A Bioinspired Soft Swallowing Robot Based on Compliant Guiding Structure. Soft Robot. 2020;7(4):491–9.
109. Esser F, Steger T, Bach D, Masselter T, Speck T. Development of Novel Foam-Based Soft Robotic Ring Actuators for a Biomimetic Peristaltic Pumping System. In 2017. p. 138–47. Available from: http://link.springer.com/10.1007/978-3-319-63537-8_12
110. Esser F, Krüger F, Masselter T, Speck T. Development and characterization of a novel biomimetic peristaltic pumping system with flexible silicone-based soft robotic ring actuators. Lect Notes Comput Sci (including Subser Lect Notes Artif Intell Lect Notes Bioinformatics). 2018;10928 LNAI:157–67.
111. Esser F, Krüger F, Masselter T, Speck T. Characterization of Biomimetic Peristaltic Pumping System Based on Flexible Silicone Soft Robotic Actuators as an Alternative for Technical Pumps [Internet]. Vol. 11556 LNAI, Lecture Notes in Computer Science (including subseries Lecture Notes in Artificial Intelligence and Lecture Notes in Bioinformatics). Springer International Publishing; 2019. 101–113 p. Available from: http://dx.doi.org/10.1007/978-3-030-24741-6_9
112. Vopalensky M, Ascanio G, Herna JA. X-ray technique for visualization of the bolus flow through an esophageal simulator. J Vis. 2021;
113. Kozu H, Nakata Y, Nakajima M, Neves MA, Uemura K, Sato S, et al. Development of a human gastric digestion simulator equipped with peristalsis function for the direct observation and analysis of the food digestion process. Food Sci Technol Res. 2014;20(2):225–33.
114. Keppler S, O'Meara S, Bakalis S, Fryer PJ, Bornhorst GM. Characterization of individual particle movement during in vitro gastric digestion in the Human Gastric Simulator (HGS). J Food Eng [Internet]. 2020;264(July 2019). Available from: https://doi.org/10.1016/j.jfoodeng.2019.07.021
115. Barros L, Retamal C, Torres H, Zúñiga RN, Troncoso E. Development of an in vitro mechanical gastric system (IMGS) with realistic peristalsis to assess lipid digestibility. Food Res Int [Internet]. 2016;90:216–25. Available from: http://dx.doi.org/10.1016/j.foodres.2016.10.049

116. Kwon J, Choi J, Lee S, Kim M, Park YK, Park DH, et al. Modelling and manufacturing of 3D-printed, patient-specific, and anthropomorphic gastric phantoms: a pilot study. Sci Rep [Internet]. 2020;10(1):1–11. Available from: https://doi.org/10.1038/s41598-020-74110-z
117. Condino S, Harada K, Pak NN, Piccigallo M, Menciassi A, Dario P. Stomach simulator for analysis and validation of surgical endoluminal robots. Appl Bionics Biomech. 2011;8(2):267–77.
118. Hashem R, Xu W, Stommel M, Cheng L. Conceptualisation and specification of a biologically-inspired, soft-bodied gastric robot. M2VIP 2016 - Proc 23rd Int Conf Mechatronics Mach Vis Pract. 2017;
119. Kawatsu C, Li J, Chung CJ. Robot Intelligence Technology and Applications 2012 [Internet]. Vol. 208, Intelligence. 2013. 623–630 p. Available from: http://link.springer.com/10.1007/978-3-642-37374-9
120. Dang Y, Cheng LK, Stommel M, Xu W. Technical requirements and conceptualization of a soft pneumatic actuator inspired by human gastric motility. M2VIP 2016 - Proc 23rd Int Conf Mechatronics Mach Vis Pract. 2017;
121. Dang Y, Devaraj H, Stommel M, Cheng LK, McDaid AJ, Xu W. Experimental Investigation into the Dynamics of a Radially Contracting Actuator with Embedded Sensing Capability. Soft Robot. 2020;7(4):478–90.
122. Han J, Chen J, Yu N, Dang Y. Active Modeling and Control of the Ring-Shaped Pneumatic Actuator: An Experimental Study. IEEE/ASME Trans Mechatronics. 2021;1–12.
123. Dang Y, Liu Y, Hashem R, Bhattacharya D, Allen J, Stommel M, et al. SoGut: A Soft Robotic Gastric Simulator. Soft Robot. 2020;8(3):273–83.
124. Hashem R, Stommel M, Cheng LK, Xu W. Design and Characterization of a Bellows-Driven Soft Pneumatic Actuator. IEEE/ASME Trans Mechatronics. 2021;26(5):2327–38.
125. Hashem R, Kazemi S, Stommel M, Cheng LK, Xu W. A Biologically Inspired Ring-Shaped Soft Pneumatic Actuator for Large Deformations. Soft Robot. 2021;00(00):1–13.
126. Kazemi S, Hashem R, Stommel M, Cheng L, Xu W. Experimental Study on the Closed-Loop Control of a Soft Ring-Shaped Actuator for In-vitro Gastric Simulator. IEEE/ASME Trans Mechatronics. 2021;1–11.
127. Granados A, Maréchal L, Barrow A, Petrou G, Norton C, Bello F. Relax and tighten—a haptics-based approach to simulate sphincter tone assessment. Lect Notes Electr Eng. 2011;432:327–33.
128. Marechal L, Granados A, Ethapemi L, Qiu S, Kontovounisios C, Norton C, et al. Modelling of anal sphincter tone based on pneumatic and cable-driven mechanisms. 2017 IEEE World Haptics Conf WHC 2017. 2017;(June):376–81.
129. Osgouei RH, Marechal L, Kontovounisios C, Bello F. Soft Pneumatic Actuator for Rendering Anal Sphincter Tone. IEEE Trans Haptics. 2020;13(1):183–90.
130. Horvath MA, Hu L, Mueller T, Hochstein J, Rosalia L, Hibbert KA, et al. An organosynthetic soft robotic respiratory simulator. APL Bioeng. 2020;4(2):1–13.
131. Lee HJ, Lee HJ, Lee JS, Kang YN, Koo JC. A built-up-type deformable phantom for target motion control to mimic human lung respiration. Rev Sci Instrum [Internet]. 2020;91(5):1–8. Available from: https://doi.org/10.1063/5.0003453
132. Liao Y, Wang L, Xu X, Chen H, Chen J, Zhang G, et al. An anthropomorphic abdominal phantom for deformable image registration accuracy validation in adaptive radiation therapy. Med Phys. 2017;44(6):2369–78.
133. Naghibi H, Dorp J Van, Abayazid M. Development of a Soft Robotics Diaphragm to Simulate Respiratory Motion. Proc IEEE RAS EMBS Int Conf Biomed Robot Biomechatronics. 2020;2020-Novem:140–5.
134. Naghibi H, Costa PAC, Abayazid M. A Soft Robotic Phantom to Simulate the Dynamic Respiratory Motion of Human Liver. Proc IEEE RAS EMBS Int Conf Biomed Robot Biomechatronics. 2018;2018-Augus:577–82.
135. Matrosic CK, Bednarz B, Culberson W. An Improved Abdominal Phantom for Intrafraction Image Guidance Validation. Phys Med Biol. 2020;2(1):1–6.
136. de Jong TL, Moelker A, Dankelman J, van den Dobbelsteen JJ. Designing and validating a PVA liver phantom with respiratory motion for needle-based interventions. Int J Comput Assist Radiol Surg [Internet]. 2019;14(12):2177–86. Available from: https://doi.org/10.1007/s11548-019-02029-6
137. Ehrbar S, Jöhl A, Kühni M, Meboldt M, Ozkan Elsen E, Tanner C, et al. ELPHA: Dynamically deformable liver phantom for real-time motion-adaptive radiotherapy treatments. Med Phys. 2019;46(2):839–50.
138. Szabała T, Rymarczyk T, Vejar A. A robotic respiration phantom with patient data synchronization for medical tomography. IOP Conf Ser Earth Environ Sci. 2020;1782(1):1–6.
139. Ranunkel O, Güder F, Arora H. Soft Robotic Surrogate Lung. ACS Appl Bio Mater. 2019;2(4):1490–7.
140. Dullius MA, Fernandes RC, Souza DN. Development and evaluation of a dynamic cardiac phantom for use in nuclear medicine. World Acad Sci Eng Technol. 2011;80:342–5.
141. Tavakoli V, Negahdar MJ, Kendrick M, Alshaher M, Stoddard M, Amini AA. A biventricular multimodal (MRI/ultrasound) cardiac phantom. Proc Annu Int Conf IEEE Eng Med Biol Soc EMBS. 2012;3187–90.
142. Gomes-Fonseca J, Morais P, Queirós S, Veloso F, Pinho ACM, Fonseca JC, et al. Personalized dynamic phantom of the right and left ventricles based on patient-specific anatomy for echocardiography studies - Preliminary results. 2018 IEEE 6th Int Conf Serious Games Appl Heal SeGAH 2018. 2018;1–7.
143. Krakovich A, Zaretsky U, Moalem I, Naimushin A, Rozen E, Scheinowitz M, et al. A new cardiac phantom for dynamic SPECT. J Nucl Cardiol [Internet]. 2020; Available from: https://doi.org/10.1007/s12350-020-02028-0
144. Hjertaas JJ, Matre K. A left ventricular phantom for 3D echocardiographic twist measurements. Biomed Tech. 2019;65(2):209–18.
145. Vannelli C, Moore J, McLeod J, Ceh D, Peters T. Dynamic heart phantom with functional mitral and aortic valves. Med Imaging 2015 Image-Guided Proced Robot Interv Model. 2015;9415.
146. Azar T, McLennan S, Walsh M, Angeles J, Kövecses J, Jaramillo T, et al. Dynamic Left Atrioventricular Phantom Test Bed Emulating Mitral Valve Motion. J Med Devices, Trans ASME. 2020;14(3).
147. Wood PW, Gibson PH, Becher H. Three-dimensional echocardiography in a dynamic heart phantom: Comparison of five different methods to measure chamber volume using a commercially available software. Echo Res

Pract. 2014;1(2):51–60.
148. Hvid R, Jensen JA, Bo Stuart M, Traberg MS. Validation Platform for Development of Computational Fluid Dynamics of Intra-Cardiac Blood-Flow. IEEE Int Ultrason Symp. 2019;868–71.
149. Zhu Y, Luo XY, Gao H, McComb C, Berry C. A numerical study of a heart phantom model. Int J Comput Math [Internet]. 2014;91(7):1535–51. Available from: https://doi.org/10.1080/00207160.2013.854337
150. Liu H, Yan J, Zhou Y, Li H, Li C. A novel dynamic cardiac simulator utilizing pneumatic artificial muscle. Proc Annu Int Conf IEEE Eng Med Biol Soc EMBS. 2013;715–8.
151. Chen CC, Shen TY, Peterson CB, Hung GU, Pan T. Comparison of ejection fraction calculation between CT and SPECT at high heart rate: A dynamic cardiac phantom study. J Nucl Cardiol [Internet]. 2020;28(1):311–6. Available from: https://doi.org/10.1007/s12350-019-01991-7
152. Thompson NA, Hsiao-wecksler ET. A soft robotic simulator for transeptal puncture training. Proc Des Med Devices Conf. 2021;5–8.
153. Gulbulak U, Ertas A. Finite Element Driven Design Domain Identification of a Beating Left Ventricular Simulator. Bioengineering. 2019;
154. Park C, Fan Y, Hager G, Yuk H, Singh M, Rojas A, et al. An organosynthetic dynamic heart model with enhanced biomimicry guided by cardiac diffusion tensor imaging. 2020;5(38):1–28.
155. Fuhrer R, Schumacher CM, Zeltner M, Stark WJ. Soft iron/silicon composite tubes for magnetic peristaltic pumping: Frequency-dependent pressure and volume flow. Adv Funct Mater. 2013;23(31):3845–9.
156. Mao G, Wu L, Fu Y, Chen Z, Natani S, Gou Z, et al. Design and Characterization of a Soft Dielectric Elastomer Peristaltic Pump Driven by Electromechanical Load. IEEE/ASME Trans Mechatronics. 2018;23(5):2132–43.
157. Schumacher CM, Loepfe M, Fuhrer R, Grass RN, Stark WJ. 3D printed lost-wax casted soft silicone monoblocks enable heart-inspired pumping by internal combustion. R Soc Chem. 2014;
158. Loepfe M, Schumacher CM, Stark WJ. Design, performance and reinforcement of bearing-free soft silicone combustion-driven pumps. Ind Eng Chem Res. 2014;53(31):12519–26.
159. Roche ET, Wohlfarth R, Overvelde JTB, Vasilyev N V., Pigula FA, Mooney DJ, et al. A bioinspired soft actuated material. Adv Mater. 2013;26(8):1200–6.
160. Mac Murray BC, Xintong A, Robinson SS, van Meerbeek IM, O'Brien KW, Zhao H, et al. Poroelastic Foams for Simple Fabrication of Complex Soft Robots. Adv Mater. 2015;27:6334–40.
161. Zhou Y, Jiang W, Cao L, Wang C, Zhang C, Liu H. Design and analysis of a novel bionic cardiac simulator. 2018 IEEE Int Conf Inf Autom ICIA 2018. 2018;1245–50.
162. Weisson EH, Fittipaldi M, Concepcion CA, Pelaez D, Grace L, Tse DT. Automated Noncontact Facial Topography Mapping, 3-Dimensional Printing, and Silicone Casting of Orbital Prosthesis. Am J Ophthalmol. 2020 Dec;220:27–36.
163. Eo MY, Cho YJ, Nguyen TTH, Seo MH, Kim SM. Implant-supported orbital prosthesis: a technical innovation of silicone fabrication. Int J Implant Dent. 2020 Dec;6(1).
164. Otto IA, Capendale PE, Garcia JP, de Ruijter M, van Doremalen RFM, Castilho M, et al. Biofabrication of a shape-stable auricular structure for the reconstruction of ear deformities. Mater Today Bio. 2021 Jan 1;9.
165. Mannoor MS, Jiang Z, James T, Kong YL, Malatesta KA, Soboyejo WO, et al. 3D printed bionic ears. Nano Lett. 2013 Jun 12;13(6):2634–9.
166. Zhou G, Jiang H, Yin Z, Liu Y, Zhang Q, Zhang C, et al. In Vitro Regeneration of Patient-specific Ear-shaped Cartilage and Its First Clinical Application for Auricular Reconstruction. EBioMedicine. 2018 Feb 1;28:287–302.
167. Tang P, Song P, Peng Z, Zhang B, Gui X, Wang Y, et al. Chondrocyte-laden GelMA hydrogel combined with 3D printed PLA scaffolds for auricle regeneration. Mater Sci Eng C. 2021 Nov 1;130.
168. Lee JM, Sultan MT, Kim SH, Kumar V, Yeon YK, Lee OJ, et al. Artificial auricular cartilage using silk fibroin and polyvinyl alcohol hydrogel. Int J Mol Sci. 2017 Aug 4;18(8).
169. Pane S, Mazzocchi T, Iacovacci V, Ricotti L, Menciassi A. Smart implantable artificial bladder: An integrated design for organ replacement. IEEE Trans Biomed Eng. 2021;68(7):2088–97.
170. Al Adem KM, Bawazir SS, Hassen WA, Khandoker AH, Khalaf K, McGloughlin T, et al. Implantable Systems for Stress Urinary Incontinence. Ann Biomed Eng. 2017;45(12):2717–32.
171. Lucarini G, Mazzocchi T, Marziale L, Ricotti L, Menciassi A. Magnetically-controlled artificial urinary sphincters for severe urinary incontinence. IEEE Int Conf Biomed Robot Biomechatronics. 2018;1242–7.
172. Hached S, Trigui A, Loutochin O, Garon A, Corcos J, Sawan M. Novel electromechanic artificial urinary sphincter. IEEE/ASME Trans Mechatronics. 2016;21(2):945–55.
173. Weiss FM, Deyhle H, Kovacs G, Müller B. Designing micro- and nanostructures for artificial urinary sphincters. Electroact Polym Actuators Devices 2012. 2012;8340.
174. Valerio M, Jichlinski P, Dahlem R, Tozzi P, Mundy AR. Experimental evaluation of an electromechanical artificial urinary sphincter in an animal model. BJU Int. 2013;112(4):337–43.
175. Goos M, Baumgartner U, Löhnert M, Thomusch O, Ruf G. Experience with a new prosthetic anal sphincter in three coloproctological centres. BMC Surg. 2013;13(1).
176. Gregorcyk SG. The current status of the Acticon® Neosphincter. Clin Colon Rectal Surg. 2005;18(1):32–7.
177. Zellmer T, MacDonald W. Palpable abdominal mass and recurrent fecal incontinence due to failure of artificial bowel sphincter. Radiol Case Reports [Internet]. 2019;14(1):66–8. Available from: https://doi.org/10.1016/j.radcr.2018.08.024
178. Ke L, Yan GZ, Liu H, Jiang PP, Liu ZQ, Wang YB, et al. A novel artificial anal sphincter system in an in vitro and in vivo experiment. Int J Artif Organs. 2014;37(3):253–63.
179. Luo Y, Higa M, Amae S, Takagi T, Yambe T, Okuyama T, et al. Preclinical development of SMA artificial anal sphincters. Minim Invasive Ther Allied Technol. 2009;15(4):241–5.
180. Luo Y, Takagi T, Amae S, Wada M, Yambe T, Kamiyama T, et al. Shape Memory Alloy Artificial Muscles for Treatments of Fecal Incontinence. Mater Trans. 2004;45(2):272–6.
181. Tsukada H, Matsuda S, Inoue H, Ikada Y, Osada H.

Comparison of bioabsorbable materials for use in artificial tracheal grafts. Interact Cardiovasc Thorac Surg. 2009;8(2):225–9.
182. Xu Y, Guo Y, Li Y, Huo Y, She Y, Li H, et al. Biomimetic Trachea Regeneration Using a Modular Ring Strategy Based on Poly(Sebacoyl Diglyceride)/Polycaprolactone for Segmental Trachea Defect Repair. Adv Funct Mater. 2020;30(42).
183. Mansfield EG, Greene VK, Auguste DT. Patterned, tubular scaffolds mimic longitudinal and radial mechanics of the neonatal trachea. Acta Biomater [Internet]. 2016;33:176–82. Available from: http://dx.doi.org/10.1016/j.actbio.2016.01.034
184. Boazak EM, Benson JM, Auguste DT. R- and Z-Axis Patterned Scaffolds Mimic Tracheal Circumferential Compliance and Longitudinal Extensibility. ACS Biomater Sci Eng. 2017;3(12):3222–9.
185. Park JH, Jung JW, Kang HW, Joo YH, Lee JS, Cho DW. Development of a 3D bellows tracheal graft: Mechanical behavior analysis, fabrication and an in vivo feasibility study. Biofabrication. 2012;4(3).
186. Park JH, Hong JM, Ju YM, Jung JW, Kang HW, Lee SJ, et al. A novel tissue-engineered trachea with a mechanical behavior similar to native trachea. Biomaterials [Internet]. 2015;62:106–15. Available from: http://dx.doi.org/10.1016/j.biomaterials.2015.05.008
187. Chua M, Chui C-K, Chng C-B, Lau D. Carbon Nanotube-Based Artificial Tracheal Prosthesis. IEEE Nanotechnol Mag. 2013;7:27–31.
188. Chua M, Chui CK, Teo C, Lau D. Patient-specific carbon nanocomposite tracheal prosthesis. Int J Artif Organs. 2015;38(1):31–8.
189. Chua C.h M, Chui CK, Rai B, Lau D.p D. Development of a patient specific artificial tracheal prosthesis: Design, mechanical behavior analysis and manufacturing. In: Proceedings of the Annual International Conference of the IEEE Engineering in Medicine and Biology Society, EMBS. 2013. p. 6236–9.
190. Kim SH, Lee HR, Yu SJ, Han ME, Lee DY, Kim SY, et al. Hydrogel-laden paper scaffold system for origami-based tissue engineering. Proc Natl Acad Sci U S A. 2015;112(50):15426–31.
191. Jung SY, Lee SJ, Kim HY, Park HS, Wang Z, Kim HJ, et al. 3D printed polyurethane prosthesis for partial tracheal reconstruction: A pilot animal study. Biofabrication [Internet]. 2016;8(4):1–10. Available from: http://dx.doi.org/10.1088/1758-5090/8/4/045015
192. Orizondo RA, Cardounel AJ, Kormos R, Sanchez PG. Artificial Lungs: Current Status and Future Directions. Curr Transplant Reports [Internet]. 2019 Dec 11;6(4):307–15. Available from: http://link.springer.com/10.1007/s40472-019-00255-0
193. Kniazeva T, Hsiao JC, Charest JL, Borenstein JT. A microfluidic respiratory assist device with high gas permeance for artificial lung applications. Biomed Microdevices. 2011;13(2):315–23.
194. Matharoo H, Dabaghi M, Rochow N, Fusch G, Brash J, Fusch C, et al. Stainless steel reinforced composite silicone membrane and its integration into microfluidic oxygenators for high performance gas exchange. 21st Int Conf Miniaturized Syst Chem Life Sci MicroTAS 2017. 2020;014107:425–6.
195. Potkay JA. A high efficiency micromachined artificial lung. TRANSDUCERS 2009 - 15th Int Conf Solid-State Sensors, Actuators Microsystems. 2009;2234–7.
196. Potkay JA, Magnetta M, Vinson A, Cmolik B. Bio-inspired, efficient, artificial lung employing air as the ventilating gas. Lab Chip. 2011;11(17):2901–9.
197. Hoganson DM, Pryor HI, Bassett EK, Spool ID, Vacanti JP. Lung assist device technology with physiologic blood flow developed on a tissue engineered scaffold platform. Lab Chip. 2011;11(4):700–7.
198. Dharia A, Abada E, Feinberg B, Yeager T, Moses W, Park J, et al. Silicon Micropore-Based Parallel Plate Membrane Oxygenator. Artif Organs. 2018;42(2):166–73.
199. Thompson AJ, Ma LJ, Plegue TJ, Potkay JA. Design Analysis and Optimization of a Single-Layer PDMS Microfluidic Artificial Lung. IEEE Trans Biomed Eng. 2019;66(4):1082–93.
200. Lee J, Kung M, Kung H, Mockros L. Microchannel Technologies for Artificial Lungs(3) Open Rectangular Channels. ASAIO J (American Soc Artif Intern Organs 1992). 2011;54:390.
201. Rieper T, Müller C, Reinecke H. Novel scalable and monolithically integrated extracorporeal gas exchange device. Biomed Microdevices. 2015;17(5):1–10.
202. Bashkin JS, Heim J, Prahlad H, Kornbluh R, Pelrine R, Elefteriades J, et al. Medical Device Applications of Dielectric Elastomer- Based Artificial Muscles. Proceedings of the Materials and Processes for Medical Devices Conferences. 2007. 242–247 p.
203. Cohrs NH, Petrou A, Loepfe M, Yliruka M, Shumacher CM, Kohll AX, et al. A Soft Total Artificial Heart - First Concept Evaluation on a Hybrid Mock Circulation. Artif Organs. 2017;
204. Guex LG, Jones LS, Kohll AX, Walker R, Meboldt M, Falk V, et al. Increased Longevity and Pumping Performance of an Injection Molded Soft Total Artificial Heart. Soft Robot. 2020;00(00):1–6.
205. Kohll AX, Cohrs NH, Walker R, Petrou A, Loepfe M, Daners MS, et al. Long-Term Performance of a Pneumatically Actuated Soft Pump Manufactured by Rubber Compression Molding. Soft Robot. 2019;6(2):206–13.
206. Cafarelli A, Losi P, Salgarella AR, Barsotti MC, Di Cioccio IB, Foffa I, et al. Small-caliber vascular grafts based on a piezoelectric nanocomposite elastomer: Mechanical properties and biocompatibility. J Mech Behav Biomed Mater [Internet]. 2019;97(December 2018):138–48. Available from: https://doi.org/10.1016/j.jmbbm.2019.05.017
207. Ohlmann L, Mohammadi H. Soft robotic in the construction of prosthetic heart valve: a novel approach. J Med Eng Technol [Internet]. 2020;44(2):76–81. Available from: https://doi.org/10.1080/03091902.2020.1723728
208. Amiri Moghadam AA, Jang SJ, Caprio A, Liu J, Singh HS, Min JK, et al. Using Soft Robotic Technology to Fabricate a Proof-of-Concept Transcatheter Tricuspid Valve Replacement (TTVR) Device. Adv Mater Technol. 2019;4(4):1–9.
209. Amiri Moghadam AA, Alaie S, Gharaie S, Nath SD, Vawda S, Al'Aref SJ, et al. Toward Development of Inflatable Stents with Application in Endovascular Treatments. Adv Funct Mater. 2018;28(51).
210. Hong SY, Lee YH, Park H, Jin SW, Jeong YR, Yun J, et al. Stretchable Active Matrix Temperature Sensor Array of Polyaniline Nanofibers for Electronic Skin. Adv Mater. 2016;28(5):930–5.

211. An R, Zhang X, Han L, Wang X, Zhang Y, Shi L, et al. Healing, flexible, high thermal sensitive dual-network ionic conductive hydrogels for 3D linear temperature sensor. Mater Sci Eng C [Internet]. 2020;107(September 2019). Available from: https://doi.org/10.1016/j.msec.2019.110310
212. Zhan Z, Lin R, Tran VT, An J, Wei Y, Du H, et al. Paper/Carbon Nanotube-Based Wearable Pressure Sensor for Physiological Signal Acquisition and Soft Robotic Skin. ACS Appl Mater Interfaces. 2017;9(43):37921–8.
213. Tie J, Rong L, Liu H, Wang B, Mao Z, Zhang L, et al. An autonomously healable, highly stretchable and cyclically compressible, wearable hydrogel as a multimodal sensor. Polym Chem. 2020;11(7):1327–36.
214. Kim CC, Lee HH, Oh KH, Sun JY. Highly stretchable, transparent ionic touch panel. Science (80-). 2016;353(6300):682–7.
215. Park S, Shin BG, Jang S, Chung K. Three-Dimensional Self-Healable Touch Sensing Artificial Skin Device. ACS Appl Mater Interfaces. 2019;12(3):3953–60.
216. Shin W, Kim JS, Choi HJ, Kim H, Park S, Lee HJ, et al. 3D Antidrying Antifreezing Artificial Skin Device with Self-Healing and Touch Sensing Capability. Macromol Rapid Commun. 2021;42(9):1–9.
217. Guo H, Bai M, Wen C, Liu M, Tian S, Xu S, et al. A Zwitterionic-Aromatic Motif-Based ionic skin for highly biocompatible and Glucose-Responsive sensor. J Colloid Interface Sci [Internet]. 2021;600:561–71. Available from: https://doi.org/10.1016/j.jcis.2021.05.012
218. Lei Z, Zhu W, Zhang X, Wang X, Wu P. Bio-Inspired Ionic Skin for Theranostics. Adv Funct Mater. 2020;31(8):1–9.
219. Li J, Wang Y, Liu L, Xu S, Liu Y, Leng J, et al. A Biomimetic Soft Lens Controlled by Electrooculographic Signal. Adv Funct Mater. 2019 Sep 1;29(36).
220. Perez-Guagnelli E, Jones J, Tokel AH, Herzig N, Jones B, Miyashita S, et al. Characterization, Simulation and Control of a Soft Helical Pneumatic Implantable Robot for Tissue Regeneration. IEEE Trans Med Robot Bionics. 2020;2(1):94–103.
221. Perez-Guagnelli ER, Nejus S, Yu J, Miyashita S, Liu Y, Damian DD. Axially and Radially Expandable Modular Helical Soft Actuator for Robotic Implantables. Proc - IEEE Int Conf Robot Autom. 2018;4297–304.
222. Yan D, Bruns TM, Wu Y, Zimmerman LL, Stephan C, Cameron AP, et al. Ultracompliant Carbon Nanotube Direct Bladder Device. Adv Healthc Mater. 2019;8(20):1–11.
223. Hassani FA, Gammad GGL, Mogan RP, Ng TK, Kuo TLC, Ng LG, et al. Design and Anchorage Dependence of Shape Memory Alloy Actuators on Enhanced Voiding of a Bladder. Adv Mater Technol. 2018;3(1):1–12.
224. Hassani FA, Peh WYX, Gammad GGL, Mogan RP, Ng TK, Kuo TLC, et al. A 3D Printed Implantable Device for Voiding the Bladder Using Shape Memory Alloy (SMA) Actuators. Adv Sci. 2017;4(11):1–10.
225. Arab Hassani F, Jin H, Yokota T, Someya T, Thakor N V. Soft sensors for a sensing-actuation system with high bladder voiding efficiency. Sci Adv. 2020;6(18):2–10.
226. Yang X, An C, Liu S, Cheng T, Bunpetch V, Liu Y, et al. Soft Artificial Bladder Detrusor. Adv Healthc Mater. 2018;7(6):1–9.
227. Hu L, Saeed M, Manisha S, Roche E. An implantable ventilator augments inspiration in an in vivo porcine model. Res Sq. 2021;1–17.
228. Options M, Varela CE, Fan Y, Roche ET. Optimizing Epicardial Restraint and Reinforcement Following Myocardial Infarction : Moving Towards. 2019;(Lv).
229. Bannerman D, Pascual-Gil S, Radisic M. An optimal gel patch for the injured heart. Nat Biomed Eng. 2019;3(8):592–3.
230. Gu H, Bertrand T, Boehler Q, Chautems C, Vasilyev N V, Nelson BJ. Magnetically Active Cardiac Patches as an Untethered , Non-Blood Contacting Ventricular Assist Device. 2021;2000726:6–11.
231. Kongahage D, Ruhparwar A, Foroughi J. High Performance Artificial Muscles to Engineer a Ventricular Cardiac Assist Device and Future Perspectives of a Cardiac Sleeve. Adv Mater Technol. 2021;6(5).
232. Mac Murray BC, Futran CC, Lee J, O'Brien KW, Amiri Moghadam AA, Mosadegh B, et al. Compliant Buckled Foam Actuators and Application in Patient-Specific Direct Cardiac Compression. Soft Robot. 2018;5(1):99–108.
233. Roche ET, Horvath MA, Alazmani A, Galloway KC, Vasilyev N V., Mooney DJ, et al. Design and fabrication of a soft robotic direct cardiac compression device. In: Proceedings of the ASME Design Engineering Technical Conference. 2015.
234. Obiajulu SC, Roche ET, Pigula FA, Walsh CJ. Soft pneumatic artificial muscles with low threshold pressures for a cardiac compression device. In: Proceedings of the ASME Design Engineering Technical Conference. 2013.
235. Roche ET, Horvath MA, Wamala I, Alazmani A, Song SE, Whyte W, et al. Soft robotic sleeve supports heart function. Sci Transl Med. 2017;9(373):1–12.
236. Horvath MA, Varela CE, Dolan EB, Whyte W, Monahan DS, Payne CJ, et al. Towards Alternative Approaches for Coupling of a Soft Robotic Sleeve to the Heart. Ann Biomed Eng. 2018;46(10):1534–47.
237. Bautista-Salinas D, Hammer PE, Payne CJ, Wamala I, Saeed M, Thalhofer T, et al. Synchronization of a Soft Robotic Ventricular Assist Device to the Native Cardiac Rhythm Using an Epicardial Electrogram. J Med Devices, Trans ASME. 2020;14(3):1–8.
238. Park E, Mehandru N, Beltran TL, Kraus E, Holland D, Polygerinos P, et al. An intraventricular soft robotic pulsatile assist device for right ventricular heart failure. J Med Devices, Trans ASME. 2014;8(2).
239. Payne CJ, Wamala I, Bautista-Salinas D, Saeed M, Van Story D, Thalhofer T, et al. Soft robotic ventricular assist device with septal bracing for therapy of heart failure. Sci Robot. 2017;2(12).
240. Horvath MA, Wamala I, Rytkin E, Doyle E, Payne CJ, Thalhofer T, et al. An Intracardiac Soft Robotic Device for Augmentation of Blood Ejection from the Failing Right Ventricle. Ann Biomed Eng. 2017;45(9):2222–33.
241. Gharaie SH, Amir Moghadam AA, Al'Aref SJ, Caprio A, Alaie S, Zgaren M, et al. A Proof-of-Concept Demonstration for a Novel Soft Ventricular Assist Device. J Med Devices, Trans ASME. 2019;13(2).